Clim Dyn
DOI 10.1007/s00382-017-3832-5

Statistical link between external climate forcings and modes of ocean variability

Abdul Malik[1,2] · **Stefan Brönnimann**[1,2] · **Paolo Perona**[3]

Received: 6 December 2016 / Accepted: 24 July 2017

Abstract In this study we investigate statistical link between external climate forcings and modes of ocean variability on inter-annual (3-year) to centennial (100-year) timescales using de-trended semi-partial-cross-correlation analysis technique. To investigate this link we employ observations (AD 1854–1999), climate proxies (AD 1600–1999), and coupled Atmosphere-Ocean-Chemistry Climate Model simulations with SOCOL-MPIOM (AD 1600–1999). We find robust statistical evidence that Atlantic multi-decadal oscillation (AMO) has intrinsic positive correlation with solar activity in all datasets employed. The strength of the relationship between AMO and solar activity is modulated by volcanic eruptions and complex interaction among modes of ocean variability. The observational dataset reveals that El Niño southern oscillation (ENSO) has statistically significant negative intrinsic correlation with solar activity on decadal to multi-decadal timescales (16–27-year) whereas there is no evidence of a link on a typical ENSO timescale (2–7-year). In the observational dataset, the volcanic eruptions do not have a link with AMO on a typical AMO timescale (55–80-year) however the long-term datasets (proxies and SOCOL-MPIOM output) show that volcanic eruptions have intrinsic negative correlation with AMO on inter-annual to multi-decadal timescales. The Pacific decadal oscillation has no link with solar activity, however, it has positive intrinsic correlation with volcanic eruptions on multi-decadal timescales (47–54-year) in reconstruction and decadal to multi-decadal timescales (16–32-year) in climate model simulations. We also find evidence of a link between volcanic eruptions and ENSO, however, the sign of relationship is not consistent between observations/proxies and climate model simulations.

Keywords Atlantic multi-decadal oscillation · Pacific decadal oscillation · El Niño southern oscillation · Solar activity · Volcanic eruptions · De-trended semi-partial-cross-correlation analysis

1 Introduction

The Atlantic multi-decadal oscillation (AMO), Pacific decadal oscillation (PDO), and El-Niño southern oscillation (ENSO) are persistent modes of ocean variability which play a substantial role in global and regional climate variability and dynamics. These modes of ocean variability can have significant impacts on African and Asian monsoons (e.g., Joly and Voldoire 2009; Kumar et al. 2006; Zhang and Delworth 2006), cause severe droughts over parts of America (e.g., McCabe et al. 2004; Mo and Schemm 2008; Jiang et al. 2013), and modulate the hurricane activity (e.g., Zhang and Delworth 2006). Understanding the drivers or modulating factors of these ocean modes can greatly enhance our capability in predicting the regional and global climate on different timescales. Several efforts have been undertaken to comprehend the effects of external climate forcings (e.g., solar activity, volcanic eruptions, CO_2, and aerosols) on theses ocean modes. Nevertheless the question

✉ Abdul Malik
abdul.malik@giub.unibe.ch

[1] Oeschger Centre for Climate Change Research, University of Bern, 3012 Bern, Switzerland

[2] Institute of Geography, University of Bern, 3012 Bern, Switzerland

[3] Institute for Infrastructure and Environment, School of Engineering, The University of Edinburgh, Edinburgh EH9 3JL, UK

Published online: 31 July 2017

still remains: can external forcings drive or significantly modulate these modes of ocean variability?

The driving factors of AMO are unclear and currently a focus of research. Inter-annual to multidecadal scale Sea Surface Temperature (SST) variations exist in the Atlantic Ocean (Otterå et al. 2010) where AMO exhibits itself as a prominent multidecadal scale (55–80 years) oscillation between warm and cold phases of SSTs (Knight et al. 2006; Wei and Lohmann 2012). Recent studies using reconstruction dataset (see, Knudsen et al. 2014) and climate model simulations (see, Stenchikov et al. 2009; Otterå et al. 2010) indicate that external forcing factors i.e. solar activity and volcanic eruptions can drive the AMO. Knudsen et al. 2014 and Otterå et al. 2010 showed that after termination of the little ice age (LIA) the combined solar and volcanic forcing leads the AMO by ~5 years. Jiang et al. (2015) using proxy reconstruction dataset showed that SSTs in the northern North Atlantic are linked with solar activity in the past 4000 years. Booth et al. (2012) using an Earth system climate model showed that anthropogenic aerosols and volcanic activity can explain 76% multi-decadal variance of north Atlantic SSTs over the period AD 1860–2005. Can a coupled Atmosphere-Ocean-Chemistry climate model simulate the relationship between external forcings and AMO as found by the previous studies?

Observational and climate model based studies suggest the influence of external climate forcings on ENSO on inter-annual and multidecadal timescales. In general, studies show a negative correlation between ENSO and solar activity on inter-annual and multidecadal timescales (e.g., Mehta and Lau 1997; Kodera 2005; Mann et al. 2005; Meehl et al. 2009; Narashima and Bhattacharyya 2010). In contrast to these studies, on multidecadal timescale, Fan et al. (2009) using climate model simulations found a positive correlation between solar activity and Niño3 index which indicate uncertainty in their relationship. The proxy based studies (e.g., Adams et al. 2003) show an El-Niño like pattern in equatorial Pacific Ocean after volcanic eruptions. However, the response of equatorial Pacific SSTs to volcanic eruption is not consistent among climate models as some simulate an El-Niño like response (e.g., Ohba et al. 2013; Maher et al. 2015; Pausata et al. 2015) whereas others show a La-Niña like response (e.g. McGregor and Timmermann 2011; Zanchettin et al. 2012). The contradicting findings of Fan et al. (2009), McGregor and Timmermann (2011), and Zanchettin et al. (2012) compared to other studies indicate that the response of ENSO to external forcings is inconsistent among climate models and needs to be further investigated.

The North Pacific SSTs also have two distinct modes of variability i.e. inter-annual and decadal (Yeh and Kirtman 2003). The decadal mode, PDO, is the leading principal component of SSTs in the north Pacific with periodicities 15–25 and 50–70 years (e.g., Mantua and Hare 2002). The inter-annual mode of north Pacific SSTs simultaneously correlates with tropical Pacific inter-annual SST variability whereas the decadal mode leads the tropical Pacific decadal SST variability by 5–7 years (Yeh and Kirtman 2003). Newman et al. (2003, 2016) found that PDO depends on ENSO on all timescales. There are several other studies which indicate interaction between the PDO and ENSO (e.g., Zhang et al. 1996; Barnett et al. 1999; Pierce et al. 2000; Fedorov and Philander 2000, 2001; Vimont et al. 2001, 2003a, b; Schneider and Cornuelle 2005; Newman 2007). Similarly, there are studies which show a link of AMO with PDO (see, D'Orgeville and Peltier 2007; Zhang and Delworth 2007; Wu et al. 2011; Kucharski et al. 2015) and ENSO (see, Dong and Sutton 2002, 2007; Dong et al. 2006; Timmermann et al. 2005, 2007; Goswami et al. 2006; Sutton and Hodson 2007; Kucharski et al. 2011; Frauen and Dommenget 2012; Kang et al. 2014; Kayano and Capistrano 2014; McGregor et al. 2014). It should be investigated whether a complex interaction between modes of ocean variability affects their relationship, if exists, with external forcings.

In the present work we investigate the statistical link between modes of ocean variability and external climate forcings using De-trended Semi-partial Cross-Correlation Analysis (DSPCCA). Recently Yuan et al. (2015) developed De-trended Partial-Cross-Correlation Analysis (DPCCA) technique to analyse correlation between two time series which are correlated to other signals as well. We extend DPCCA to DSPCCA using the method proposed by Kim (2015). The DPCCA is a combination of two statistical techniques i.e. De-trended Cross-Correlation Analysis (DCCA), and Partial-Cross-Correlation Analysis (PCCA). The DPCCA can analyse a complex system of several interlinked variables. Often, climatic variables subjected to cross correlation are simultaneously teleconnected with several other variables and it is not easy to isolate their intrinsic/direct relationship. In the presence of non-stationarities and periodic background signals the calculated correlation coefficients can be overestimated or inaccurate (Yuan et al. 2015). The DCCA has the advantage over traditional correlation analysis that it accurately measures the correlation coefficient between two variables even if any level of non-stationarity (or local trend) is present (Kristoufek 2015). Another advantage of the DCCA is that it can be used to study the relationship between two variables on different time scales (Dong et al. 2014). The DPCCA method removes the non-stationarities (using DCCA) as well as partials out the influence of background signals (using PCCA) from the variables being cross correlated and thus gives a robust estimate of correlation.

In a complex scenario where AMO, PDO, and ENSO have simultaneous/lead/lagged interactions with each other

on different timescales, and where external forcings also play their role, it urges to investigate the intrinsic (true) relationship between the ocean modes of variability and external climate forcings. Can the factors, for instance the PDO and ENSO, modulate the strength of the relationship between the AMO and external forcings on different timescales? We investigate the extrinsic (in the presence of potential modulating factors) as well as the intrinsic (in the absence of potential modulating factors) correlation between modes of ocean variability (AMO, PDO, and Niño3) and external forcings (solar activity and volcanic eruptions) on inter-annual (3-year) to centennial (100-year) timescales. We employ DCCA, and DSPCCA techniques on observational (AD 1854–1999) and proxy (AD 1600–1999) datasets, and coupled Atmosphere-Ocean-Chemistry (AOCCM) climate model simulations with SOCOL MPIOM to answer following questions: (1) is there any link between modes of ocean variability and external forcings, (2) at what timescales these modes of ocean variability are linked to external forcings and (3) can the complex interaction among the ocean modes of variability modulate their relationship with external forcings?

The paper is organized as follows. Section 2 presents the data and methods. The results are demonstrated in Sect. 3. Finally, the discussion and conclusions are summarized in Sect. 4.

2 Data and methods

2.1 Model description

A coupled atmosphere–ocean-chemistry climate model is important to reasonably simulate the influence of solar activity and volcanic eruptions on atmosphere and ocean (see, Kodera 2004, 2005; Meehl et al. 2009; Reichler et al. 2012). Therefore, the present study employs four transient simulations (i.e., L1, L2, M1, and M2) carried out with the coupled Atmosphere–Ocean-Chemistry Climate Model (AOCCM) SOCOL-MPIOM over the period AD 1600–1999 with all major forcings. The model has a horizontal grid of T31 (≈3.75°×3.75°) with 39 irregular vertical pressure levels (L39) up to 0.01 hPa. The ocean component (MPIOM) of the model has horizontal resolution of 3° which varies between 22 km (Greenland) and 350 km (Tropical Pacific). The model was nudged to Quasi-Biennial Oscillation (QBO) reconstruction according to Brönnimann et al. (2007). All four simulations were run with different ocean initial condition. The model was forced with Total Solar Irradiance (TSI) reconstruction of Shapiro et al. (2011) which is considerably different in terms of amplitude from the other TSI reconstructions (e.g., Lean et al. 1995; Krivova et al. 2011). The simulations L1 and L2 were carried out with strong irradiance amplitude (6 W/m^2) of 1 W/m^2 forcing, whereas M1 and M2 were carried out with medium irradiance amplitude (3 W/m^2) of 0.5 W/m^2 forcing. The calculation time step for dynamical processes is 15 min and 144 min for the ocean component. The atmosphere–ocean coupling takes place every 24 h (Anet et al. 2013a, b; Muthers et al. 2014).

2.2 Datasets

2.2.1 Gridded SST datasets

Two gridded SST reconstructions, in addition to the model output, i.e. the Extended Reconstructed Sea Surface Temperature version 4 (ERSSTv4) (Liu et al. 2014; Huang et al. 2015, 2016) over the period AD 1854–1999, and SST reconstruction by Mann et al. (2009) over the period AD 1600–1999 (hereafter, Mann-Recon) are used in the present study. The ERSSTv4 has global coverage with a horizontal resolution of 2°×2°. The ERSSTv4 data is provided by the NOAA/OAR/ESRL PSD, Boulder, Colorado, USA (http://www.esrl.noaa.gov/psd/). Mann–Recon is a multiproxy reconstruction based on more than a 1000 tree rings, ice cores, corals, sediments, and other proxies. The Mann–Recon does not show inter-annual variability and is meaningful only at inter-decadal to longer timescales (Mann et al. 2009). Therefore, we use a slightly modified version of this reconstruction by Bhend et al. (2012) (hereafter, Mann–ReconMod). The Mann-Recon was inter- and extra-polated to T63 (approximately 1.85°×1.85°) and then superimposed with a seasonal cycle and ENSO-dependent intra-annual variability. The seasonal cycle was derived from HadISST1.1 of Rayner et al. (2003) and ENSO-dependent intra-annual variability was obtained by regressing Niño3.4 index of Cook et al. (2008) onto HadISST1.1 (Bhend J, personal communication, 2015).

2.2.2 AMO index

The AMO index for ERSSTv4 (hereafter AMO-ERSST), Mann–ReconMod (hereafter, AMO-Mann), and simulated datasets (L1, L2, M1, and M2) is calculated by employing the method of Enfield et al. (2001). First we calculate global (60°N–60°S) SST anomalies relative to AD 1951–1980, and then average, de-trend, and low-pass filter (11-year running mean) these anomalies over the north Atlantic region (0°N–60°N, 0°W–80°W).

We also use AMO reconstruction by Gray et al. (2004) over the period AD 1600–1990 (hereafter, AMO-Gray) downloaded from the web site of NOAA National Centers for Environmental Information (NCEI; http://www.ncdc.noaa.gov/data-access/paleoclimatology-data/datasets/tree-ring). The AMO-Gray is based on tree-ring chronologies

from eastern North America, Europe, Scandinavia, North Africa, and the Middle East (Gray et al. 2004). The AMO reconstruction by Mann et al. (2009) and Gray et al. (2004) are the best amongst the available historical AMO reconstructions (Knudsen et al. 2014). All the AMO indices used in this study are shown in Fig. 1a.

2.2.3 PDO index

The PDO index based on ERSSTv4 over the period AD 1854–1999 is downloaded from the web site of NCEI (hereafter PDO-ERSST; http://www.ncdc.noaa.gov/teleconnections/pdo/). For Mann–ReconMod, and model, the PDO index is calculated using the method of Mantua et al. (1997) as described by Lapp et al. (2012). First, the residual SSTs are calculated by subtracting the global(60°N–60°S) monthly SST anomalies (relative to 1961–1990) from the SST anomalies over the north Pacific region (20°N–60°N, 120°E–90°W). The empirical orthogonal function (EOF) analysis is performed for these residuals and the first principal component is taken as the PDO index. The PDO index calculated from Mann–ReconMod will be referred to as PDO-Mann. Another PDO reconstruction by Shen et al. (2006) over the period AD 1600–1990 is used in this study (hereafter, PDO-Shen). This PDO reconstruction is based on proxy reconstruction of summer rainfall of eastern China extracted from historical documentary records over the period AD 1470–2000 (Shen et al. 2006). In the present study the PDO-Shen is preferred over the PDO reconstruction by MacDonald and Case (2005) because PDO-Shen shows better correlation (0.67) with ERSSTv4 than the PDO reconstruction by MacDonald (0.26) over the period AD 1854–1999. All the PDO indices used in this study are shown in Fig. 1b.

2.2.4 Niño3 index

The Niño3 index is calculated by averaging the SSTs over the Niño3 region (5°N–5°S, 150°W–90°W) for the months of June–September (JJAS). To cover the area between 5°N–5°S and 150°W–90°W the SSTs for ERSSTv4, Mann-ReconMod, and model were re-gridded to 1°×1° using bilinear interpolation. The Niño3 index calculated from ERSSTv4 and Mann–ReconMod will be referred to as Niño3-ERSST and Niño3-Mann, respectively. We also use the Niño3 reconstruction by Cook et al. (2008) over the period AD 1600–1990 (hereafter Niño3-Cook). This Niño3 reconstruction (December–February, DJF) is based on tree-ring chronologies from Texas and Mexico. After 1979 this reconstruction is appended with instrumental data (Cook et al. 2008). All the Niño3 indices used in this study are shown in Fig. 1c.

The model evaluation for AMO, PDO, and Niño3 was performed by Malik et al. (2017) which showed that the

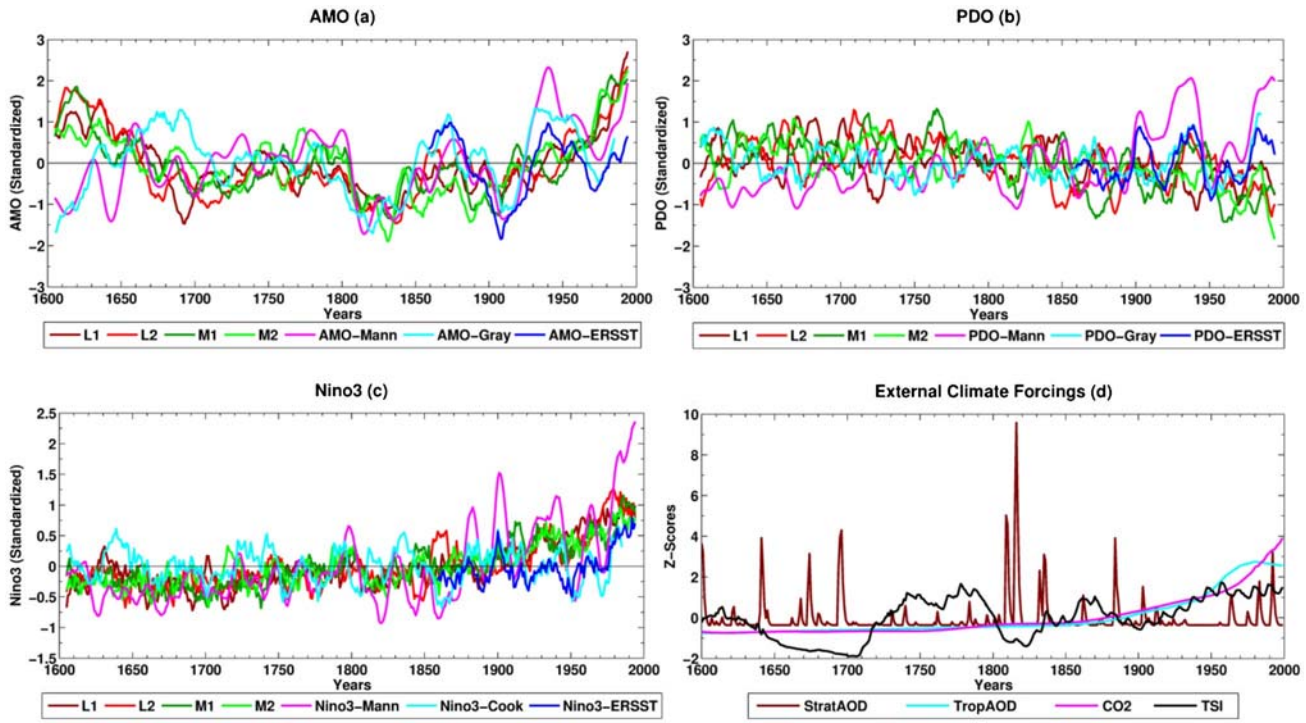

Fig. 1 Filtered (11-year running mean) observed, proxy based, and simulated **a** AMO index, **b** PDO index and **c** Niño3 index. **d** Unfiltered external climate forcings used as input in AOCCM SOCOL-MPIOM and for statistical analyses

model has reasonable skill for simulating the spatiotemporal patterns and periodicities of these ocean modes of variability.

2.2.5 External climate forcings

The external climate forcing datasets used in the present research are Proxy for volcanic forcing such as stratospheric aerosol optical depth (StratAOD) in the visible band (Arfeuille et al. 2014), tropospheric aerosol optical depth (TropAOD) obtained from CAM3.5 simulations with a bulk aerosol model run by fixed SSTs and CMIP emission over the period AD 1850–2000 (S. Bauer, personal communication, 2011), CO_2 (Ramaswamy et al. 2001), and TSI by Shapiro et al. (2011). All these external forcings are shown in Fig. 1d. Note that strong volcanic activity occurred during the minima of solar activity i.e. Maunder minimum (AD ~ 1650–1710) and Dalton minimum (AD ~ 1800–1840) which can mask the solar effect on climatic variables (Breitenmoser et al. 2012). Thus, for studying the influence of solar activity it is important to remove the effects of volcanic eruptions from the climatic variable being analyzed.

2.3 Methods

In order to study the extrinsic and intrinsic correlations between modes of ocean variability and external forcings we employ the DCCA and DSPCCA techniques on inter-annual (3-year) to centennial (100-year) timescales. The DCCA method was proposed by Podobnik and Stanley (2008) and a DCCA coefficient was introduced by Zebende (2011) (Dong et al. 2014) which ranges between −1 and +1. Several examples of using DCCA coefficients are available in a range of fields (see, Hajian and Movahed 2010; He and Chen 2011; Vassoler and Zebende 2012; Kang et al. 2013; Marinho et al. 2013; Dong et al. 2014). We have implemented the DCCA and DPCCA algorithm as described by Yuan et al. (2015) and further extend it to DSPCCA according to Kim (2015). The mathematical algorithm for DPCCA is expressed in following steps:

We suppose there is n number of random walks or time series

$$\overline{x_i^1}, \overline{x_i^2}, \overline{x_i^3}, \ldots, \overline{x_i^n} \text{ where, } i = 1, 2, 3, \ldots, T \text{ (length of each time series)} \quad (1)$$

We build n integrated profiles, Z_k^j, for these n time series as

$$Z_k^j = \sum_{i=1}^{k} x_i^j, \text{ where, } j = 1, 2, 3, \ldots, n, \text{ and } k = 1, 2, 3, \ldots, T \quad (2)$$

If ts is a time scale at which we want to calculate DCCA and DPCCA, each integrated profile Z_k^j is divided into T − ts overlapping boxes such that each box having ts + 1 observations starts at i and ends at i + ts. A local trend $Z_{k,i}^j$ $(i \leqslant k \leqslant i + ts)$ is determined in each overlapping box i of an integrated profile Z_k^j by fitting a polynomial of an appropriate order. The order of polynomial depends on the type of trend present in the time series.

Residuals or de-trended walks are defined by subtracting the local trend $Z_{k,i}^j$ from the original integrated profile, Z_k^j, such that

$$R^j_{(i-1)(ts+1)+(k-i+1)} = Z_k^j - Z_{k,i}^j \quad (3)$$

Where, the de-trended walk R_i^j for each time series will contain $l = 1, 2, 3, \ldots, (T - ts)(ts + 1)$ elements.

Calculate the co-variance between any two de-trended walks as

$$F^2_{j1,j2}(ts) = \frac{\sum_{l=1}^{(T-ts)(ts+1)} R_l^{j1} R_l^{j2}}{(T - ts)(ts - 1)} \text{ where } j1, j2 = 1, 2, 3, \ldots, n \quad (4)$$

The covariance matrix for n de-trended walks can be defined as

$$F^2(ts) = \begin{bmatrix} F^2_{1,1}(ts) & F^2_{1,2}(ts) & \ldots & F^2_{1,n}(ts) \\ F^2_{2,1}(ts) & F^2_{2,2}(ts) & \ldots & F^2_{2,n}(ts) \\ \vdots & \vdots & \ldots & \vdots \\ F^2_{n,1}(ts) & F^2_{n,2}(ts) & \ldots & F^2_{n,n}(ts) \end{bmatrix} \quad (5)$$

The correlation coefficient between time series $\overline{x_i^{j1}}$, and $\overline{x_i^{j2}}$ can be calculated as

$$\rho_{j1,j2}(ts) = \frac{F^2_{j1,j2}(ts)}{F_{j1,j1}(ts) \cdot F_{j2,j2}(ts)} \quad (6)$$

The correlation matrix is calculated as

$$\rho(ts) = \begin{bmatrix} \rho_{1,1}(ts) & \rho_{1,2}(ts) & \ldots & \rho_{1,n}(ts) \\ \rho_{2,1}(ts) & \rho_{2,2}(ts) & \ldots & \rho_{2,n}(ts) \\ \vdots & \vdots & \ldots & \vdots \\ \rho_{n,1}(ts) & \rho_{n,2}(ts) & \ldots & \rho_{n,n}(ts) \end{bmatrix} \quad (7)$$

Calculate the inverse of correlation matrix $\rho(ts)$ as

$$IC(ts) = \rho^{-1}(ts) = \begin{bmatrix} IC_{1,1}(ts) & IC_{1,2}(ts) & \ldots & IC_{1,n}(ts) \\ IC_{2,1}(ts) & IC_{2,2}(ts) & \ldots & IC_{2,n}(ts) \\ \vdots & \vdots & \ldots & \vdots \\ IC_{n,1}(ts) & IC_{n,2}(ts) & \ldots & IC_{n,n}(ts) \end{bmatrix} \quad (8)$$

From the inverse correlation matrix, 휚$^{-1}$(ts), DPCCA can be obtained as

$$휚_{DPCCA}(j1,j2;ts) = \frac{-IC_{j1,j2}(ts)}{IC_{j1,j1}(ts)\cdot IC_{j2,j2}(ts)} \quad (9)$$

By Kim (2015) the DPCCA can be extended to DSPCCA as

$$휚_{DSPCCA}(j1,j2;ts) = \frac{휚_{DPCCA}(j1,j2;ts)F_{j1,j1}(ts)}{IC_{j1,j1}(ts) - IC_{j1,j2}(ts)IC^{-1}_{j2,j2}(ts)IC_{j2,j1}(ts)} \quad (10)$$

This gives the DSPCCA coefficient that ranges between −1 and +1.

For removing non-stationarities a 1st order polynomial is fitted in each overlapping box and then DCCA and DSPCCA are calculated on inter-annual (3-year) to centennial (100-year) timescales without any smoothing or filtering of the data. The significance of DCCA and DSPCCA coefficients is tested using Monte Carlo simulation. We generate 5000 surrogate samples for each original time series employing the Corrected Amplitude Adjusted Fourier Transform (CAAFT) algorithm. The surrogate data generated from CAAFT algorithm retains the same autocorrelation and amplitude distribution as the original time series. A 1st order Autoregressive (AR1) model is fitted to original time series. From this AR1 model, 5000 realizations are generated and transformed to match the amplitude distribution, cumulative density function, and linear correlations of the original time series (Kugiumtzis 2000). Some other algorithms (e.g., AAFT; and IAAFT: Iterative AAFT) for surrogate data generation also exist but here we prefer to use CAAFT as it is a more conservative approach for significance testing (Kugiumtzis 2000). The code for the CAAFT algorithm was downloaded from the MathWorks website (http://ch.mathworks.com/matlabcentral/fileexchange/4612-surrogate-data). The correlation coefficient critical values are calculated at 90 and 95% significance.

In the present research we use three ocean modes (AMO, PDO, and Niño3) and four external forcings (TSI, CO_2, TropAOD, and StratAOD). For DCCA and DSPCCA analyses four curves are plotted in corresponding figures (e.g., Fig. 2a). In these figures the DCCA represents that the effects of none of the background signals (potential modulating factors) are removed (shown as black curve) whereas the DSPCCA-AllVar represents that the effects of all background signals (potential modulating factors) are removed from the variables (AMO, PDO, and Niño3) being cross-correlated with TSI/StratAOD. The blue curve shows that the effects of remaining two ocean modes, other than the ocean mode being cross-correlated, are not removed. The green curve shows that the effects of remaining three external forcings, other than the external forcing being cross-correlated, are not removed. For instance, if AMO and TSI are cross-correlated, then the blue curve [DSPCCA-PDO. Nino3(no)] indicates that the effects of remaining three external climate forcings (CO_2, TropAOD and StratAOD) are removed but it could not remove the remaining two ocean modes (PDO and Niño3) from AMO. Similarly, the green curve [DSPCCA-CO2.TropAOD.StratAOD(no)] indicates that the effects of remaining two ocean modes (PDO and Niño3) are removed but could not remove the remaining three external forcings (CO_2, TropAOD and StratAOD). Thus the blue curve gives us an idea that how the remaining two ocean modes together can modulate the relationship between variables subjected to cross-correlation whereas the green curve tells us how the remaining three external forcings can modulate the relationship between the variables subjected to cross-correlation. Further, in subsequent sections DCCA and DSPCCA-AllVar will be referred to as extrinsic and intrinsic relationship/correlation, respectively. Note that DSPCCA does not remove the effect of any variable from TSI and StratAOD.

3 Results

3.1 Modes of ocean variability and solar activity

3.1.1 Atlantic multidecadal oscillation

Using DCCA and DSPCCA, the relationship between AMO and TSI is examined for observations (Fig. 2a), proxies (Fig. 2b–e), climate model simulations (Fig. 3a–d), and results are summarized in Table 1. The intrinsic relationship between AMO and TSI is calculated by removing the effects of PDO, Niño3, CO_2, TropAOD, and StratAOD from AMO (red curve). All datasets, except proxies and M1, show statistically significant positive intrinsic relationship between AMO and TSI on decadal to multidecadal timescales over the period AD 1600–1999. Proxies and M1 do show positive intrinsic relationship between AMO and TSI but the relationship between them is not statistically significant over the period AD 1600–1999/1990. The AMO-ERSST has statistically significant (95%) positive intrinsic (extrinsic) relationship with TSI on 19–80-year (24–100-year) timescales with DSPCCA (DCCA) coefficients varying between 0.39 and 0.73 (0.41–0.81). The maximum value of intrinsic correlation is 0.73 at 43-year timescale. The DCCA coefficients (black curve) are lower than that of DSPCCA-AllVar which indicates that the background signals (PDO, Niño3, CO_2, TropAOD, and StratAOD) can modulate the intrinsic relationship between

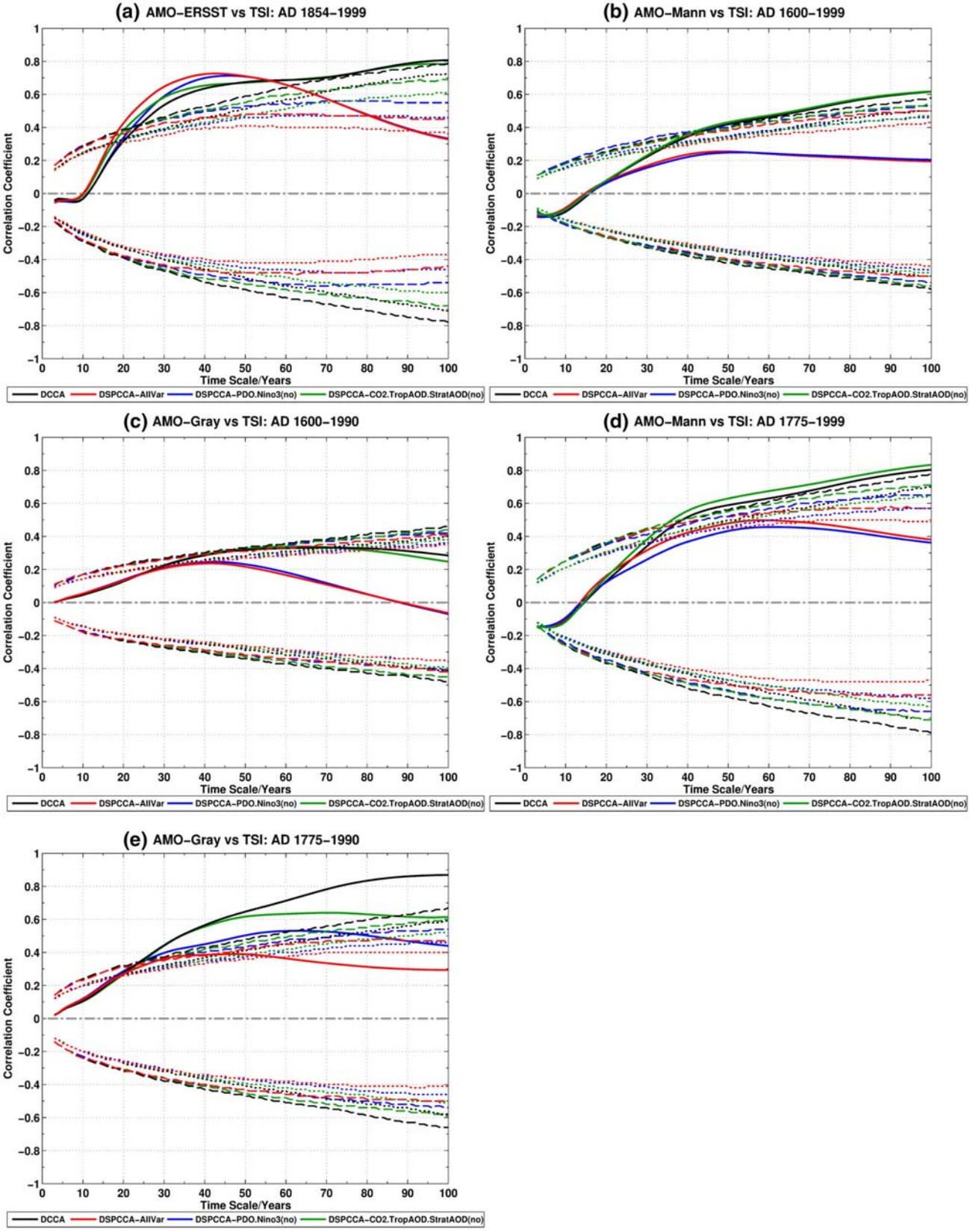

Fig. 2 DCCA and DSPCCA coefficients between AMO and TSI for **a** AMO-ERRST; AD 1854–1999, **b** AMO-Mann; AD 1600–1999, **c** AMO-Gray; AD 1600–1990, **d** AMO-Mann; AD 1775–1999 and **e** AMO-Gray; AD 1775–1990. The dotted (dashed) lines indicate the correlation coefficient critical values at 90% (95%) significance. Section 2.3 for explanation of legends

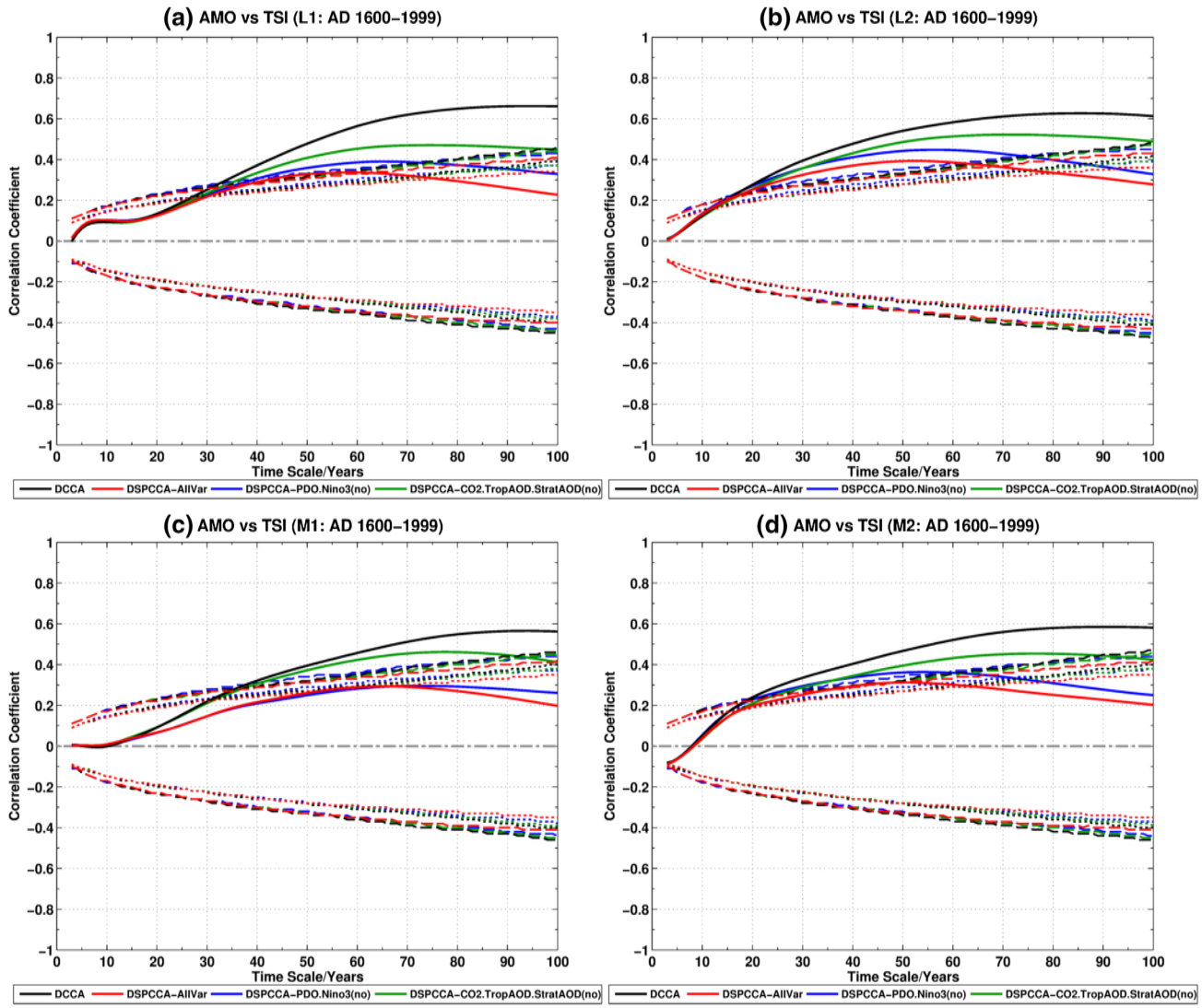

Fig. 3 DCCA and DSPCCA coefficients between AMO and TSI calculated over the time period AD 1600–1999 for ensemble member **a** L1, **b** L2, **c** M1 and **d** M2. The dotted (dashed) lines indicate the correlation coefficient critical values at 90% (95%) significance. Section 2.3 for explanation of legends

AMO and TSI. It is obvious from the Fig. 2a that the combined effect of CO_2, TropAOD, and StratAOD strengthens the intrinsic relationship between AMO and TSI over the period AD 1854–1999 (green curve) on multidecadal to centennial timescales (≈60–100-year) whereas the interaction of PDO and Niño3 with AMO does not seem to play a considerable role (blue curve).

There are no statistically significant intrinsic correlations between AMO reconstructions (AMO-Mann: AD 1600–1999; and AMO-Gray: AD 1600–1990) and TSI on decadal to multidecadal timescales (Red curves Fig. 2b, c). However, AMO-Mann does show a statistically significant (95%) weak intrinsic negative correlation (between −0.12 and −0.13) with TSI on inter-annual timescales (3–5-year). Both AMO reconstructions show extrinsic correlations with TSI on decadal to centennial timescales. The AMO-Mann (AMO-Gray) has statistically significant positive extrinsic relationship with TSI on 43–100-year (31–71-year) with DCCA coefficients varying between 0.37 and 0.61 (0.23 and 0.33). It appears that in both reconstructions the statistically significant positive extrinsic correlations between AMO and TSI are due to the presence of other external forcings, i.e., CO_2, TropAOD, and StratAOD (green curve) as both black and green curves follow the same path. However, in both reconstructions the intrinsic relation of AMO and TSI does not seem to be affected by the presence of PDO and Niño3 as red and blue curves follow the same path over the whole time period analyzed.

The AMO reconstructions (AMO-Mann and AMO-Gray) show a robust link with TSI over the period AD

Table 1 Statistically significant DCCA and DSPCCA coefficients with corresponding timescales calculated between AMO and TSI

Dataset	DCCA (90%) (95%) (timescale: coefficients)	DSPCCA (90%) (95%) (timescale: coefficients)
ERSSTv4	21–100: 0.34 to 0.81	17–91: 0.32 to 0.73
	24–100: 0.41 to 0.81	19–80: 0.39 to 0.73
Mann	3–7: −0.13 to −0.14; 36–100: 0.29 to 0.61	3–6: −0.12 to −0.13; 39–67: 0.42 to 0.50*
	3–6: −0.13 to −0.14; 43–100: 0.37 to 0.61	3–5: −0.12 to −0.13
Gray	31–71: 0.23 to 0.33	19–57: 0.26 to 0.39**
	–	–
L1	27–100: 0.21 to 0.66	31–74: 0.23 to 0.34
	32–100: 0.27 to 0.66	42–55: 0.30 to 0.33
L2	13–100: 0.17 to 0.62	12–78: 0.16 to 0.39
	16–100: 0.22 to 0.62	17–64: 0.22 to 0.39
M1	31–100: 0.23 to 0.56	–
	36–100: 0.28 to 0.56	–
M2	16–100: 0.18 to 0.59	20–64: 0.19 to 0.31
	20–100: 0.23 to 0.59	37–50: 0.28 to 0.31

*DSPCCA calculated over the time period AD 1775–1999

**DSPCCA calculated over the time period AD 1775–1990

1775–1999/1990. The reason for this may be that the quality of reconstructions before AD 1775 is not as good as after AD 1775. The atmospheric and oceanic conditions during the little ice age were different than present day conditions. Thus, the calibration of the proxies to the instrumental data before AD 1775 may be partly invalid (Knudsen et al. 2014). Recently Knudsen et al. (2014) claimed that the combined solar and volcanic forcing played a significant role in driving the AMO after AD 1775. They observed an abrupt change in correlation of combined solar and volcanic forcing with AMO-Mann, and AMO-Gray around AD 1750 and AD 1775, respectively. Further, they found that AMO-Gray is negatively correlated with combined solar and volcanic forcing before AD ~1775, however both reconstructed AMO indices (AMO-Mann, and AMO-Gray) show a positive correlation after AD 1775. The DCCA and DSPCCA coefficients between both AMO reconstructions and TSI over the period AD 1775–1999 show different results compared to the entire period AD 1600–1999 (Fig. 2d–e). Both AMO reconstructions show statistically significant positive intrinsic correlations with TSI where other external forcings (CO_2, TropAOD, and StratAOD) also seem to modulate the strength of their relationship (compare, green, blue, and black curves with red curve) on multi-decadal to centennial timescales. The statistically significant (90%) intrinsic positive correlation between AMO-Mann (AMO-Gray) and TSI varies between 0.42 and 0.50 (0.26 and 0.39) on 39–67-year (19–57-year) timescales over the period AD 1775–1999 (1775–1990).

The climate model simulations (L1, L2, and M2; AD 1600–1999) also show robust evidence of the intrinsic relationship between AMO and TSI on decadal to multi-decadal timescales (red curves in Fig. 3a–d). The extrinsic relation is stronger compared to the intrinsic relation in all four model simulations (black curve). The other external forcings (CO_2, TropAOD, and StratAOD; green curves) and PDO and Niño3 (blue curves) seem to modulate the strength of the relationship between AMO and TSI (compare green and blue curves with red curve in Fig. 3a–d).

How the correlation between the AMO and TSI evolved over the time period analyzed? We investigate the temporal evolution of the relationship between AMO and TSI by using running Pearson's correlations (over 100-year moving window) (Fig. 4a). It is interesting to note that the simulated and reconstructed AMO indices show a consistent positive correlation with TSI after AD 1750. However, before AD 1750 the relationship between AMO and TSI is more variable than after AD 1750. The simulated AMO indices show a sudden dip in the strength of their correlation with TSI during the Maunder minimum (around AD ~ 1650–1710). Note that it is a period with below normal solar activity and strong volcanic eruptions (cf. Fig. 1d). The sudden decrease in the strength of correlation is more obvious for simulations with weak solar forcing (M1 and M2) than those with strong solar forcing (L1 and L2) (see, Fig. 4a).

What caused the sudden decrease in the strength of correlation between AMO and TSI during the Maunder minimum? We investigate this puzzle with the help of DCCA and DSPCCA (Fig. 4b–e). The running DCCA and DSPCCA coefficients (Piao et al. 2016) between AMO and TSI are presented in Fig. 4b–e on centennial timescale (100-year moving window). The DCCA coefficients (black curve) for all four ensemble members suddenly drop either to zero (in L1) or turn into negative (in L2, M1, and M2) during the Maunder Minimum. If we

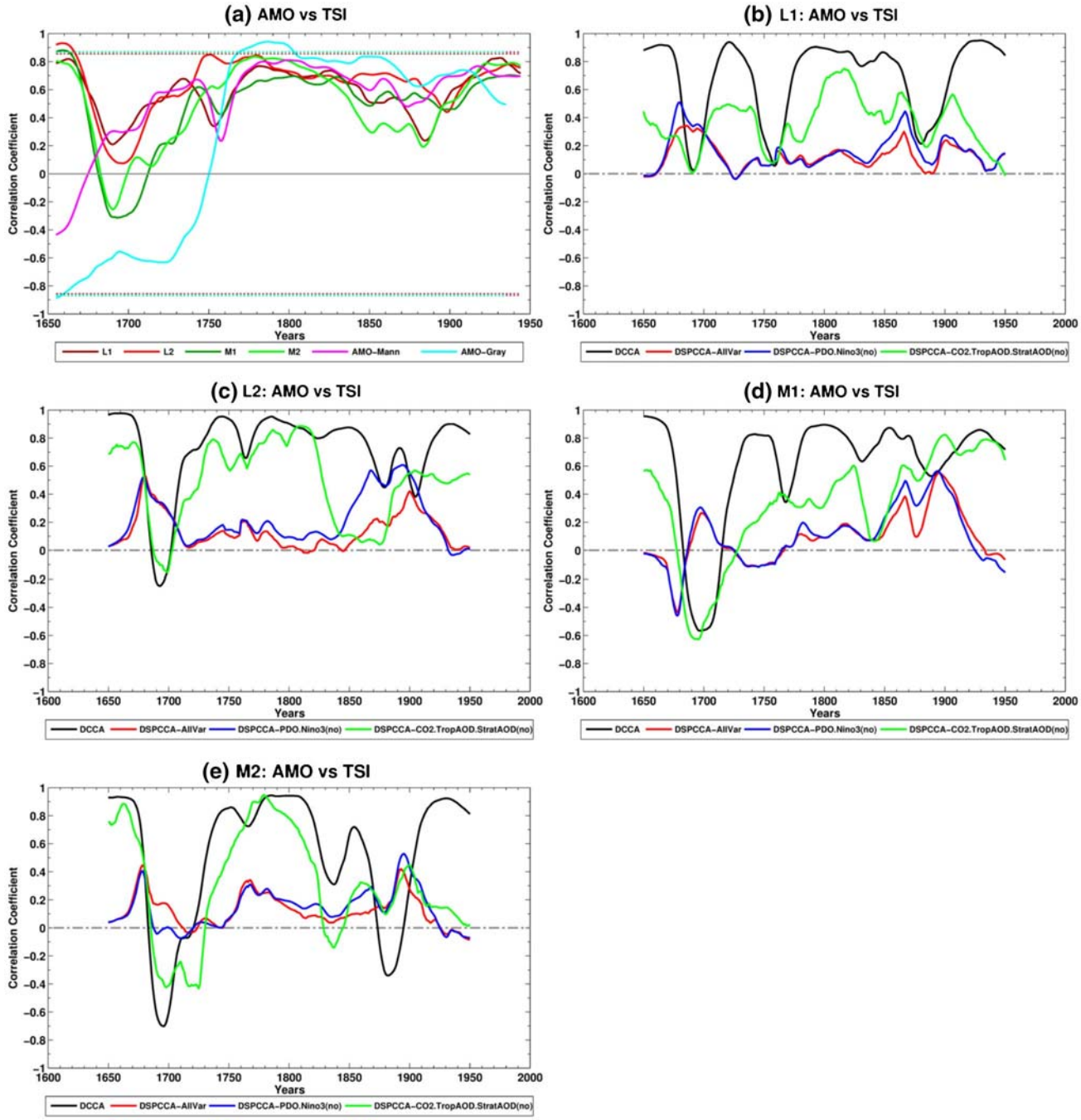

Fig. 4 Running Pearson's correlations coefficients (100-year moving window) between AMO and TSI for simulated and reconstructed datasets (**a**). Running DCCA and DSPCCA coefficients (100-year moving window) between AMO and TSI for ensemble member **b** L1, **c** L2, **d** (M1) and **e** M2. Following Knudsen et al. (2014) all datasets in **a** were smoothed (11-year moving window) before calculating the running correlations. The dotted (dashed) lines indicate the correlation coefficient critical values at 90% (95%) significance. Section 2.3 for explanation of legends

remove the influence of all potential modulating factors (CO_2, TropAOD, StratAOD, PDO, and Niño3; red curve) we do not see a sharp dip in the strength of correlation between AMO and TSI during the Maunder Minimum. A further analysis reveals that this sudden dip in strength of correlation was caused by the strong volcanic eruptions during the Maunder Minimum. If we do not remove the effects of CO_2, TropAOD, and StratAOD we observe that the DSPCCA-CO2.TropAOD.StratAOD(no) coefficients (green curve) are close to the DCCA coefficients during

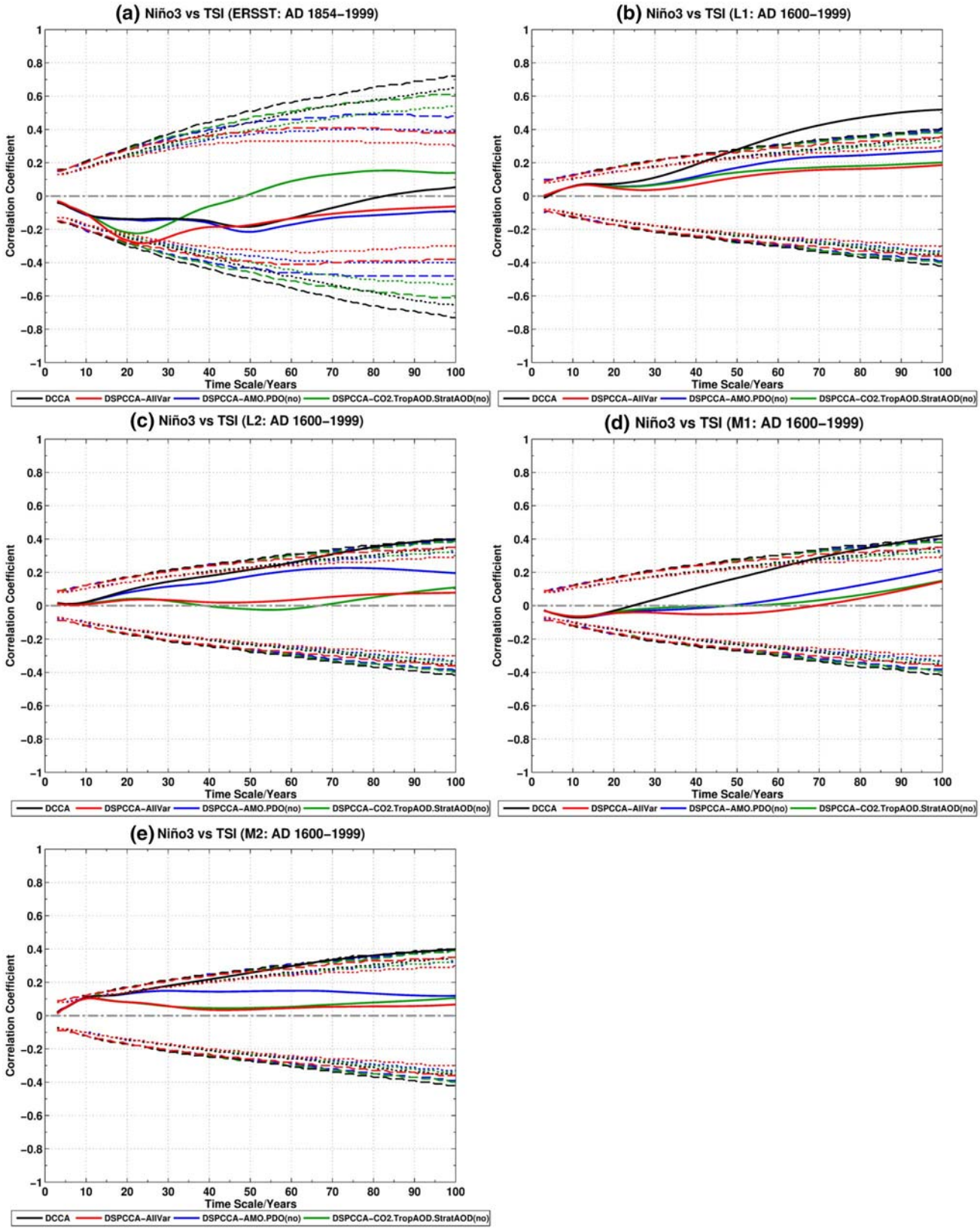

Fig. 5 DCCA and DSPCCA coefficients between Niño3 and TSI for observations (AD 1854–1999) and model simulations (AD 1600–1999) **a** Niño3-ERRST, **b** L1, **c** L2, **d** M1 and **e** M2. The dotted (dashed) lines indicate the correlation coefficient critical values at 90% (95%) significance. Section 2.3 for explanation of legends

the Maunder minimum period (compare black and green curve).

The PDO and Niño3 do not seem to play a role as their presence does not alter the intrinsic correlations between AMO and TSI during the Maunder Minimum (compare red and blue curve). In all four simulations, except L2, the blue curve mostly follows the red curve which indicates that PDO and Niño3 mostly do not affect the intrinsic relation between AMO and TSI. However, in L2 we observe considerable effect of PDO and Niño3 on intrinsic relation between AMO and TSI over the period AD 1840–1900 where blue and red curves largely deviate from each other. We conclude that strong volcanic eruptions during a prolonged (multi-decadal) solar minimum period can weaken or reverse the relationship between AMO and TSI. Also the relationship between AMO and TSI is not stationary over the time period analyzed which is partly caused by variability in PDO, ENSO, and volcanic eruptions.

3.1.2 Pacific decadal oscillation

We do not find any statistically significant DCCA and DSPCCA coefficients between PDO and TSI on any timescale in observations, proxies, and climate model simulations (not shown). The non-existence of any extrinsic and intrinsic relationship between PDO and TSI on interannual-to-centennial timescale indicates that PDO is mainly an internal mode of climate variability. Our findings are thus in agreement with the observations and climate model simulations by Newman et al. (2016), who concluded that PDO is mostly an intrinsic mode of climate variability on decadal, and decadal-to-centennial timescales. They also showed that PDO is not a single phenomenon rather results from integration of different atmospheric and oceanic processes in the tropics and north Pacific. Similarly, Schneider and Cornuelle (2005) suggested that PDO is a response of intrinsic changes in the north Pacific atmosphere, ENSO, and oceanic processes. Newman et al. (2003) also showed that PDO is dependent on ENSO on all timescales.

3.1.3 El Niño southern oscillation

Using DCCA and DSPCCA the relationship between Niño3 and TSI is examined for observations (Fig. 5a), proxies, climate model simulations (Fig. 5b–e), and the results are summarized in Table 2. The intrinsic relationship between Niño3 and TSI is calculated by removing the effects of AMO, PDO, CO_2, TropAOD, and StratAOD from Niño3 (red curve). Only the observational dataset shows intrinsic relationship between Niño3 and TSI on decadal timescales. The Niño3-ERSST has statistically significant negative intrinsic relationship with TSI on 16–27-year timescale with DSPCCA coefficients varying between −0.22 and −0.28. On a typical ENSO timescale (2–7-year) we do not see any relationship between Niño3 and TSI either intrinsically or extrinsically. The strength of the correlation between Niño3 and TSI is modulated by other external signals i.e. CO_2, TropAOD, and StratAOD (green curve) on multidecadal timescales, whereas AMO and PDO (blue curve) seem to modulate this relationship between 15 and 40-year timescales.

Table 2 Statistically significant DCCA and DSPCCA coefficients with corresponding timescales calculated between Niño3 and TSI

Dataset	DCCA (90%) (95%) (timescale: coefficients)	DSPCCA (90%) (95%) (timescale: coefficients)
ERSSTv4	–	16–27: −0.22 to −0.28
	–	–
Mann	–	–
	–	–
Cook	–	–
	–	–
L1	44–100: 0.23 to 0.52	–
	51–100: 0.27 to 0.52	–
L2	61–100: 0.26 to 0.40	–
	–	–
M1	69–100: 0.28 to 0.42	–
	93–100: 0.39 to 0.42	–
M2	31–100: 0.18 to 0.40	10: 0.10
	–	–

Both Niño3 reconstructions do not show any statistically significant evidence of the link between Niño3 and TSI (not shown). The climate model simulations also do not show statistically significant intrinsic relationship between Niño3 and TSI at any timescale. However, DCCA coefficients are statistically significant at different timescales in climate model simulations (L1: 44–100-year; L2: 61–100-year; M1: 69–100-year; M2: 31–100-year) with varying DCCA coefficients (L1: 0.23–0.52; L2: 0.26–0.40; M1: 0.28–0.42; M2: 0.18–0.40). There is a clear difference in sign of correlation between Niño3 and TSI in observations (negative sign) and climate model simulations (positive sign).

We conclude that solar activity has intrinsic relationship with ENSO on decadal to multi-decadal timescale only in observations over the period AD 1854–1999.

3.2 Modes of ocean variability and volcanic eruptions

3.2.1 Atlantic multidecadal oscillation

Using DCCA and DSPCCA the relationship between AMO and StratAOD (volcanic eruptions) is examined for observations (Fig. 6a), proxies (Fig. 6b, c), climate model simulations (Fig. 7a–d), and the results are summarized

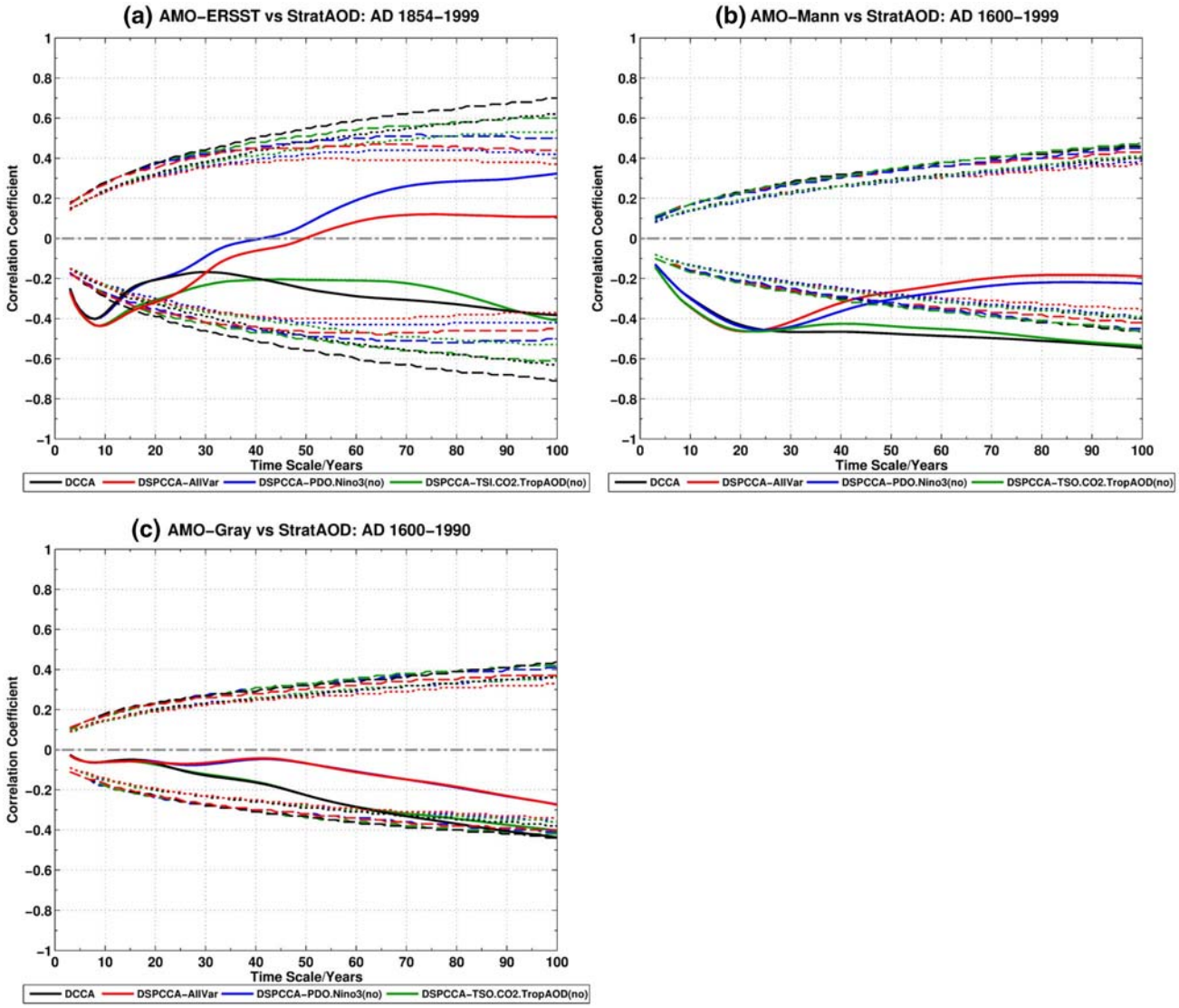

Fig. 6 DCCA and DSPCCA coefficients between AMO and StratAOD for **a** AMO-ERRST; AD 1854–1999, **b** AMO-Mann; AD 1600–1999, **c** AMO-Gray; AD 1600–1990. The dotted (dashed) lines indicate the correlation coefficient critical values at 90% (95%) significance. Section 2.3 for explanation of legends

in Table 3. The intrinsic relationship between AMO and StratAOD is calculated by removing the effects of PDO, Niño3, TSI, CO_2, and TropAOD from AMO (red curve). All datasets, except AMO-Gray, show negative intrinsic relationship between AMO and StratAOD either on inter-annual to decadal or inter-annual to multi-decadal timescales.

The AMO-ERSST has statistically significant (95%) negative intrinsic (extrinsic) relationship with StratAOD on 3–16-year (3–12-year) timescale with DSPCCA (DCCA) coefficients varying between −0.26 and −0.43 (−0.25 to −0.40). On a typical AMO timescale (55–80-year) we do not find any evidence of a link between AMO-ERSST and StratAOD.

The AMO-Mann has statistically significant (95%) negative intrinsic relationship with StratAOD on inter-annual to multi-decadal timescales (3–43-year) with DSPCCA coefficients varying between −0.14 and −0.46. The extrinsic relationship between AMO-Mann (AMO-Gray) and StratAOD is significant on 3–100-year (70–100-year) timescales with DCCA coefficients varying between −0.13 and −0.55 (−0.33 and −0.44) at 95% (90%) significance.

All four climate model simulations show statistically significant extrinsic correlation between AMO and StratAOD on inter-annual to decadal, and multi-decadal to centennial timescales (Fig. 7a–d) with varying magnitudes of DCCA coefficients. The four simulations also show the

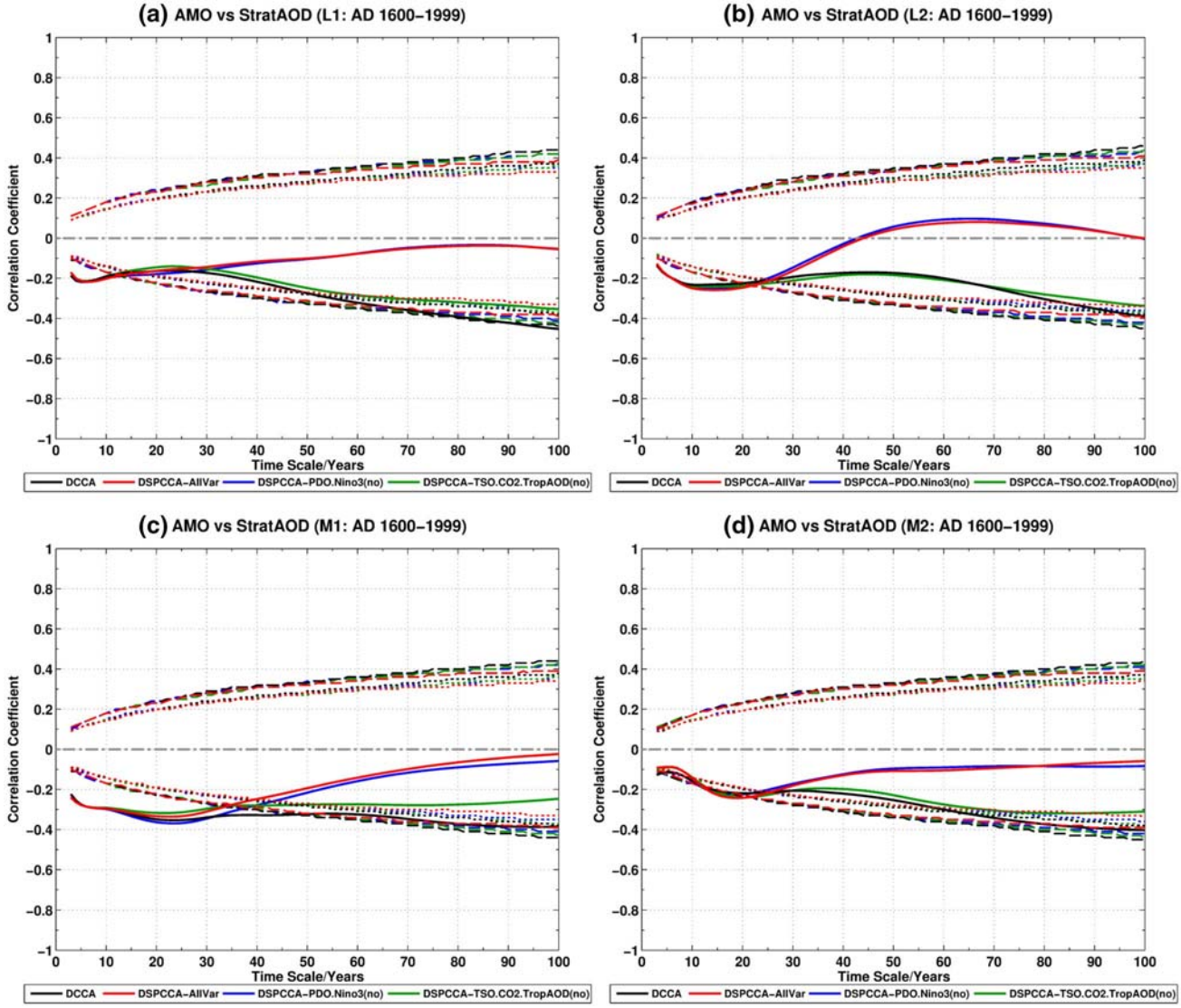

Fig. 7 DCCA and DSPCCA coefficients between AMO and StratAOD calculated over the time period AD 1600–1999 for ensemble member **a** L1, **b** L2, **c** M1 and **d** M2. The dotted (dashed) lines indicate the correlation coefficient critical values at 90% (95%) significance. Section 2.3 for explanation of legends

statistically significant intrinsic relationship on inter-annual to multi-decadal timescales.

It is evident from observational, proxy, and simulated datasets that the external forcings, i.e., CO_2, TropAOD, and TSI together can modulate the strength of intrinsic relationship between AMO and StratAOD on multi-decadal to centennial timescales (see difference between green and red curves) whereas the PDO and Niño3 together has almost no effect on the intrinsic relationship (compare red and blue curves).

We conclude that there is an intrinsic link between AMO and volcanic eruptions on inter-annual to decadal and inter-annual to multi-decadal timescales.

3.2.2 Pacific decadal oscillation

Using DCCA and DSPCCA the relationship between PDO and StratAOD (volcanic eruptions) is examined for observations (Fig. 8a), proxies (Fig. 8b), climate model simulations (Fig. 8c), and results are summarized in Table 4. The intrinsic relationship between PDO and StratAOD is calculated by removing the effects AMO, Niño3, TSI, CO_2, and TropAOD from PDO (red curve). The observational dataset indicates intrinsic (extrinsic) relationship between PDO and StraAOD only on inter-annual timescales of 3–4-year (3-year) with magnitude of correlation varying between 0.16 and 0.17 (0.15).

Table 3 Statistically significant DCCA and DSPCCA coefficients with corresponding timescales calculated between AMO and StratAOD

Dataset	DCCA (90%) (95%) (timescale: coefficients)	DSPCCA (90%) (95%) (timescale: coefficients)
ERSSTv4	3–13: −0.25 to −0.40	3–21: −0.26 to −0.43
	3–12: −0.25 to −0.40	3–16: −0.26 to −0.43
Mann	3-100: −0.13 to −0.55	3–48: −0.14 to −0.46
	3-100: −0.13 to −0.55	3–43: −0.14 to −0.46
Gray	70–100: −0.33 to −0.44	–
	–	–
L1	3–15: −0.17 to −0.22; 53–100: −0.29 to −0.45	3–16: −0.17 to −0.22
	3–12: −0.17 to −0.22; 93–100: −0.43 to −0.45	3–13: −0.17 to −0.22
L2	3–25: −0.14 to −0.23; 97–100: −0.38 to −0.39	3–25: −0.13 to −0.26
	3–19: −0.14 to −0.23	3–21: −0.13 to −0.26
M1	3-100: −0.22 to −0.39	3–39: −0.24 to −0.34
	3–48: −0.22 to −0.35	3–34: −0.24 to −0.34
M2	3–5: −0.12 to −0.13; 9–25: −0.14 to −0.22; 65–100: −0.32 to −0.40	10–25: −0.14 to −0.24
	3–4: -0.12; 12–13: −0.18 to −0.19: 15–17: -0.21	12–21: −0.18 to −0.24

The PDO-Mann shows statistically significant (90%) intrinsic relationship with StratAOD on multidecadal timescales (37–76-year) with DSPCCA coefficients varying between −0.25 and −0.34. The PDO-Shen does not show statistically significant DCCA or DSPCCA coefficients at any timescales (not shown).

In climate model simulations only the ensemble member M2 shows statistically significant (90%) intrinsic (extrinsic) relationship on 11–62-year (3–44-year) timescales with DSPCCA (DCCA) coefficients varying between −0.14 and −0.27 (−0.11 and −0.26).

There is no evidence of modulation of the relationship between PDO and StratAOD by the external forcings i.e. CO_2, TropAOD, and TSI, and AMO and Niño3 together. We conclude that PDO has a link with volcanic eruptions on inter-annual and multi-decadal timescales.

3.2.3 El Niño southern oscillation

Using DCCA and DSPCCA the relationship between Niño3 and StratAOD (volcanic eruptions) is examined for observations (Fig. 9a), proxies (Fig. 9b, c), climate model simulations (Fig. 9d), and results are also summarized in Table 5. The intrinsic relationship between Niño3 and StratAOD is calculated by removing the effects AMO, PDO,TSI, CO_2, and TropAOD from Niño3 (red curve). In the observational dataset there is statistically significant (90%) positive intrinsic relationship between Niño3 and StratAOD only on inter-annual to decadal timescales (9–14-year) with DSPCCA coefficients varying between 0.18 and 0.22.

In reconstructions the Niño3-Mann does not show any statistically significant link with StratAOD. The Niño3-Cook has statistically significant (95%) positive intrinsic (extrinsic) relationship with StratAOD on 4–26-year (4–26-year) with DSPCCA (DCCA) coefficients varying between 0.13 and 0.23 (0.13 and 0.24).

In climate model simulations only the ensemble member M1 shows statistically significant (90%) negative intrinsic relationship between Niño3 and StratAOD on decadal timescale 24–36-year with DSPCCA coefficients varying between −0.16 and −0.19. There is a clear difference in sign of relationship between model simulations (negative), and observations and reconstructions (positive).

4 Conclusions and discussion

In the present work we investigate the statistical link between external forcings and ocean modes of variability in observations, climate proxies, and coupled atmosphere-ocean-chemistry climate model simulations with SOCOL-MPIOM. We use De-trended Semi-partial-Cross-Correlation analysis technique to study the influence of Sun and volcanic eruptions on AMO, PDO, and ENSO on inter-annual to centennial timescales. We also investigate whether complex interaction between ocean modes varies their relationship with external forcings. The findings of the present research can be summarized as follows:

1. There is intrinsic positive correlation between AMO and solar activity. The strength of the relationship between AMO and solar activity is modulated by volcanic eruptions and complex interaction among ocean modes of variability. Strong volcanic eruptions during the Maunder Minimum resulted into change of strength

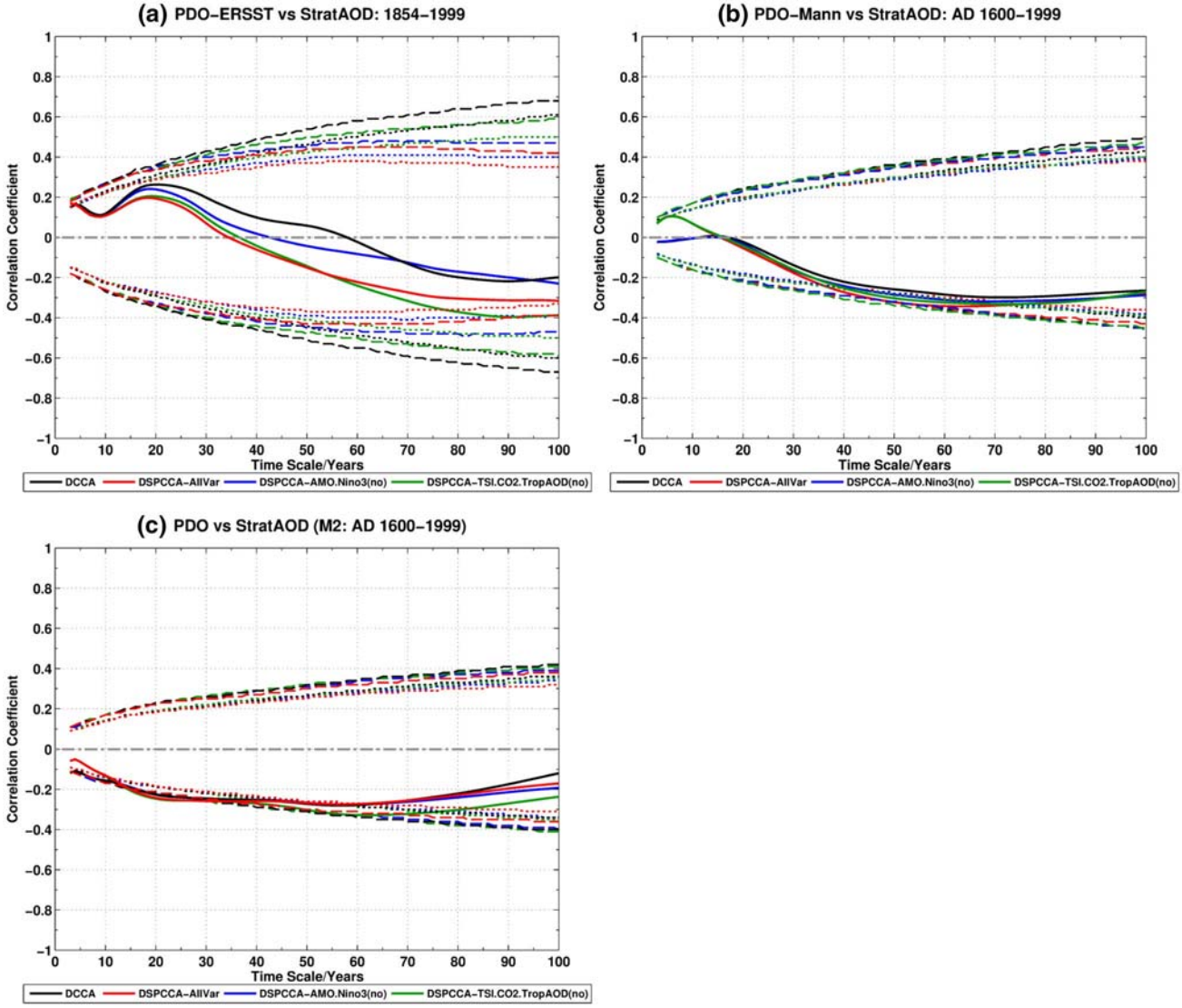

Fig. 8 DCCA and DSPCCA coefficients between PDO and StratAOD for **a** PDO-ERRST; AD 1854–1999, **b** PDO-Mann; AD 1600–1999 and **c** ensemble member L1; AD 1600–1999. The dotted (dashed) lines indicate the correlation coefficient critical values at 90% (95%) significance. Section 2.3 for explanation of legends

and sign (positive to negative) in relationship between AMO and solar activity. Thus, we posit that strong volcanic eruptions coinciding with a prolonged solar minimum period (multi-decadal) can change the strength as well as the nature of relationship between AMO and solar activity. The relationship between AMO and solar activity is non-stationary which could be partly due to volcanic eruptions and complex interaction of PDO and Niño3 with AMO, and external forcings.

2. There is an intrinsic negative correlation between AMO and volcanic eruptions. The observational dataset (AD 1854–1999) does not show a link between AMO and volcanic eruptions on a typical AMO timescale (55–80-year), however, there is evidence of a link on inter-annual to decadal timescales. In contrast to observations, the climate proxies and model simulations (AD 1600–1999) indicate negative intrinsic correlation between AMO and volcanic eruptions on inter-annual to multidecadal timescales.
3. There is no evidence of the influence of solar activity on PDO, however, we find positive intrinsic correlation between PDO and volcanic eruptions on different timescales. The PDO seems to be influenced by volcanic eruptions on multidecadal timescales (47–54-year) in Mann et al. (2009) reconstruction, and decadal to multi-decadal timescales (16–32-year) in climate model simulations. The observational dataset does not show any link between PDO and volcanic eruptions on

Table 4 Statistically significant DCCA and DSPCCA coefficients with corresponding timescales calculated between PDO and StratAOD

Dataset	DCCA (90%) (95%) (timescale: coefficients)	DSPCCA (90%) (95%) (timescale: coefficients)
ERSSTv4	3: 0.15	3–4: 0.16 to 0.17
	–	–
Mann	–	37–76: −0.25 to −0.34
	–	47–54: −0.31 to −0.33
Shen	–	–
	–	–
L1	–	–
	–	–
L2	–	–
	–	–
M1	–	–
	–	–
M2	3–44: −0.11 to −0.26	11–62: −0.14 to −0.27
	3: −0.11; 18–27: −0.21 to −0.24	16–32: −0.21 to −0.26

typical PDO timescales (15–25-year or 50–70-year) however on inter-annual timescale (3–4-year) we find a positive intrinsic relationship.

4. There is an intrinsic negative correlation between Niño3 and TSI in observations (AD 1854–1999) on decadal to multi-decadal timescales (16–27) and there is no evidence of a link on a typical ENSO timescale (2–7-year). We do not find any intrinsic relationship between Niño3 and solar activity in proxies and climate model simulations at any timescale. However, in contrast to observations, the climate model simulations show positive extrinsic relationship between Niño3 and solar activity on multi-decadal timescales. Thus, the evidence of a link between Niño3 and solar activity is not consistent among observations, climate proxies, and climate model simulations.
5. The observed Niño3 (JJAS; AD 1854–1999) and Niño3 reconstruction by Cook et al. (2008) (DJF; AD 1600–1990) indicate an El Niño like response on inter-annual to decadal time scale owing to positive intrinsic correlation between Niño3 and volcanic eruptions (9–14-year and 3–29 in observations and proxy respectively). There is a La Niña like response to volcanic eruptions in climate model simulations (AD 1600–1999) on decadal to multi-decadal timescales (24–36-year) due to a negative correlation between Niño3 and volcanic eruptions. The evidence that volcanic eruptions influence the ENSO variability is consistent among the observations, climate proxies, and model simulations but with difference in sign of correlation and timescales.

Our findings regarding influence of solar activity and volcanic eruptions on AMO are consistent with previous studies (e.g., Otterå et al. 2010; Booth et al. 2012; Knudsen et al. 2014; Jiang et al. 2015). Our observational findings that on multidecadal timescale the Niño3 has a negative correlation with solar activity are consistent with that of Mehta and Lau (1997). On multidecadal timescale the positive extrinsic correlation of Niño3 with solar activity in climate model simulations is consistent with findings of Fan et al. (2009). The inconsistent findings among observations, climate proxies, and climate model simulations still remain a puzzle and are beyond the scope of this paper. An El Niño like response of eastern equatorial Pacific SSTs to volcanic eruptions is consistent with previous proxy based findings of Adams et al. (2003). However, the atmosphere-ocean-chemistry climate model simulations show a La Niña like response of eastern equatorial Pacific SSTs to volcanic eruptions which is consistent with climate model based studies of McGregor and Timmermann (2011) and Zanchettin et al. (2012) and inconsistent with Ohba et al. (2013) and Pausata et al. (2015).

External forcings can influence the AMO through different mechanisms. The AMO and Atlantic Meridional Overturning Circulation (AMOC) are correlated. Strengthening (weakening) of the AMOC results into a warm (cold) phase of the AMO (e.g., Wei and Lohmann 2012; Zhang and Wang 2013). Several studies indicate a link between AMOC and external forcings (e.g., Otterå et al. 2010; Swingedouw et al. 2014; Pausata et al. 2015; Muthers et al. 2016). Knudsen et al. (2014) using instrumental dataset showed that the combined volcanic and solar forcing influence the AMO through AMOC. The zero time lag cross-covariance analysis of combined solar and volcanic forcings with North Atlantic SSTs showed positive covariances over most parts of the north Atlantic with relatively strong effect over the Gulf Stream and the North Atlantic Subtropical Gyre regions. With a 30-year time lag the

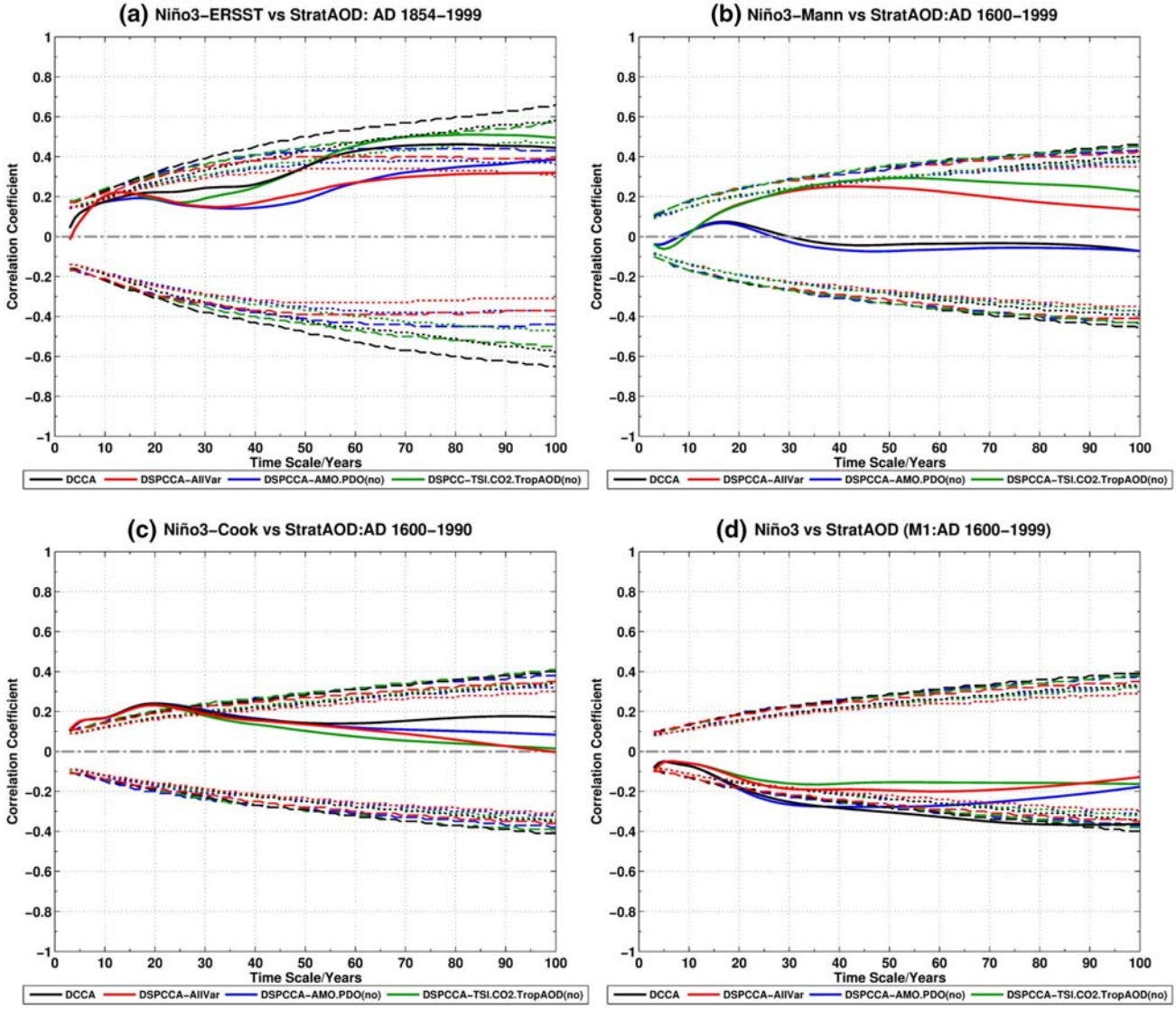

Fig. 9 DCCA and DSPCCA coefficients between Niño3 and StratAOD **a** Niño3-ERRST; AD 1854–1999, **b** Niño3-Mann; AD 1600–1999, **c** Niño3-Cook; AD 1600–1990 and **d** ensemble member L1; AD 1600–1999. The dotted (dashed) lines indicate the correlation coefficient critical values at 90% (95%) significance. Section 2.3 for explanation of legends

cross-covariances turns into negative over the North Atlantic region which is half of the ≈60-year AMO cycle. External forcings may also influence the AMO through North Atlantic oscillation (NAO). Using climate model simulations Otterå et al. (2010) showed that radiative forcing of volcanic eruptions play a considerable role in controlling the multi-decadal variability of the North Atlantic region. Volcanic eruptions induce a positive phase of NAO and strengthen the AMOC through radiative cooling. The NAO causes changes in surface air temperatures, air-sea heat fluxes, and wind stress over the North Atlantic Ocean (Visbeck et al. 2003). Positive (negative) NAO anomalies tend to occur after solar maximum (minimum) through a top-down (stratospheric response to ultraviolet solar forcing) mechanism with a lag of 0–2-year. Persistent top-down forcing of NAO also influences the SSTs (Gray et al. 2016) which subsequently may affect the AMO.

We find a robust evidence of a link between solar activity and AMO, which can have implications for hurricanes, and African and Indian monsoon whose multi-decadal variability varies in phase with AMO (see, Zhang and Delworth 2006). The Indian monsoon rainfall is positively correlated with the AMO (e.g., Joshi and Pandey 2011; Malik et al. 2017). The implication of Sun-AMO relationship for monsoon is that a period of weak solar activity can weaken the AMO strength, which can result into reduced rainfall over the African and Indian monsoon region. A decline in solar activity like Maunder minimum is predicted in the

Table 5 Statistically significant DCCA and DSPCCA coefficients with corresponding timescales calculated between Niño3 and StratAOD

Dataset	DCCA (90%) (95%) (timescale: coefficients)	DSPCCA (90%) (95%) (timescale: coefficients)
ERSSTv4	–	9–14: 0.18 to 0.22
	–	–
Mann	–	–
	–	–
Cook	3–31: 0.10 to 0.24	3–29: 0.11 to 0.23
	4–26: 0.13 to 0.24	4–26: 0.13 to 0.23
L1	–	–
	–	–
L2	–	–
	–	–
M1	17–100: −0.14 to −0.37	24–36: −0.16 to −0.19
	22–84: −0.20 to −0.37	–
M2	5–7: −0.10 to −0.11; 42–89: −0.22 to −033	–
	–	–

twenty-first century (see, Abreu et al. 2010; Lockwood 2010; Steinhilber and Beer 2013) which may have a significant impact on AMO and in turn monsoon activity. Using climate model simulations there is need to investigate that how the Sun-AMO connection during the predicted Maunder minimum can modulate the monsoon activity and other relevant climate patterns.

In the present work, we have presented all the extrinsic and intrinsic correlations with zero time lag. The calculation of time-lagged DCCA and DSPCCA is beyond the scope of this paper since their mathematical algorithm differs from that of zero time-lag (see, Chenhua 2015). Chenhua (2015) developed the algorithm for time-lagged DCCA that needs to be further extended for time-lagged DPCCA and DSPCCA. The time-lagged DCCA and DSPCCA may result into different correlation values between modes of ocean variability and external forcings, and demand a separate and detailed analysis.

Acknowledgements We acknowledge support from the Federal Commission for Scholarships for Foreign Students for the Swiss Government Excellence Scholarship (ESKAS no. 2013.0516) for the academic year(s) 2013-16/17, SNF project FUPSOL2 (CRSII2-147659), and the EC FP7 project ERA-CLIM2: 607029. We are grateful to NOAA/OAR/ESRL PSD, Boulder, Colorado, USA (http://www.esrl.noaa.gov/psd/) for providing ERSST dataset. Paolo Perona wishes to thank the Climatology Research Group at the Institute of Geography of the University of Bern for hosting him as academic guest in the Fall 2015.

References

Abreu JA, Beer J, Ferriz-Mas A (2010) Past and future solar activity from cosmogenic radionuclides. In: Cranmer RS, J. Hoeksema JT, Kohl JL (eds) SOHO-23: understanding a peculiar solar minimum. AstrSoc P 428:287–295

Adams JB, Mann ME, Ammann CM (2003) Proxy evidence for an El Niño-like response to volcanic forcing. Nature 426:274–278. doi:10.1038/nature02101

Anet JG, Muthers S, Rozanov EV, Raible CC, Peter T, Stenke A, Shapiro AI, Beer J, Steinhilber F, Brönnimann S, Arfeuille FX, Brugnara Y, Schmutz W (2013a) Forcing of stratospheric chemistry and dynamics during the Dalton Minimum. Atmos Chem Phys 13:10951–10967. doi:10.5194/acp-13-10951-2013

Anet JG, Rozanov EV, Muthers S, Peter T, Brönnimann Stefan, Arfeuille FX, Beer J, Shapiro AI, Raible CC, Steinhilber F, Schmutz WK (2013b) Impact of a potential 21st century "grand solar minimum" on surface temperatures and stratospheric ozone. Geophys Res Lett. doi:10.1002/grl.50806

Arfeuille F, Weisenstein D, Mack H, Rozanov E, Peter T, Brönnimann S (2014) Volcanic forcing for climate modeling: a new microphysics-based data set covering years 1600-present. Clim Past 10:359–375. doi:10.5194/cp-10-359-2014

Barnett TP, Pierce DW, Latif M, Dommenget D (1999) Interdecadal interactions between the tropics and midlatitudes in the Pacific basin. Geophys Res Lett 26:615–618. doi:10.1029/1999GL900042

Bhend J, Franke J, Folini D, Wild M, Brönnimann S (2012) An ensemble based approach to climate reconstructions. Clim Past 8:963–976. doi:10.5194/cp-8-963-2012

Booth BBB, Dunstone NJ, Halloran PR, Andrews T, Bellouin N (2012) Aerosols implicated as a prime driver of twentieth-century North Atlantic climate variability. Nature 484(7393):228–232. doi:10.1038/nature10946

Breitenmoser P, Beer J, Brönnimann S, Frank D, Steinhilber F, Wanner H (2012) Solar and volcanic fingerprints in tree-ring chronologies over the past 2000 years. Palaeogeogr Palaeoclimatol Palaeoecol 313–314:127–139. doi:10.1016/j.palaeo.2011.10.014

Brönnimann S, Annis JL, Vogler C, Jones PD (2007) Reconstructing the quasi-biennial oscillation back to the early 1900s. Geophys Res Lett. doi:10.1029/2007GL031354

Chenhua S (2015) Analysis of detrended time-lagged cross-correlation between two nonstationary time series. Phys Lett A 379:680–687. doi:10.1016/j.physleta.2014.12.036

Cook ER, D'Arrigo RD, Anchukaitis KJ (2008) ENSO reconstructions from long tree-ring chronologies: unifying the differences? Talk presented at a special workshop on "Reconciling ENSO Chronologies for the Past 500 Years", held in Moorea, French Polynesia on April 2–3

D'Orgeville M, Peltier WR (2007) On the Pacific Decadal Oscillation and the Atlantic Multidecadal Oscillation: might they be related? Geophys Res Lett. doi:10.1029/2007GL031584

Dong BW, Sutton RT (2002) Adjustment of the coupled ocean-atmosphere system to a sudden change in the thermohaline circulation. Geophys Res Lett. doi:10.1029/2002GL0115229

Dong BW, Sutton RT (2007) Enhancement of ENSO variability by a weakened Atlantic thermohaline circulation in coupled GCM. J Clim 20:4920–4939. doi:10.1175/JCLI4284.1

Dong BW, Sutton RT, Scaife AA (2006) Multidecadal modulation of El Niño Southern Oscillation (ENSO) variance by Atlantic Ocean sea surface temperatures. Geophys Res Lett. doi:10.1029/2006GL025766

Dong K, Zhang H, Gao Y (2014) Modeling complex system correlation using detrended cross-correlation coefficient. Math Probl Eng. doi:10.1155/2014/230537

Enfield DB, Mestas-Nunez AM, Trimble PJ (2001) The Atlantic Multidecadal Oscillation and its relationship to rainfall and river flows in the continental U.S. Geophys Res Lett 28:2077–2080. doi:10.1029/2000GL012745

Fan F, Mann ME, Ammann CM (2009) Understanding Changes in the Asian summer monsoon over the past millennium: insights from a long-term coupled model simulation. J Clim 22:1736–1748. doi:10.1175/2008JCLI2336.1

Fedorov AV, Philander SG (2000) Is El Niño changing? Science 288:1997–2002. doi:10.1126/science.288.5473.1997

Fedorov AV, Philander SG (2001) A stability analysis of tropical ocean-atmosphere interactions: bridging measurements and theory for El Niño. J Clim 14:3086–3101. doi:10.1175/1520-0442(2001)014<3086:ASAOTO>2.0.CO;2

Frauen C, Dommenget D (2012) Influences of the tropical Indian and Atlantic Oceans on the predictability of ENSO. Geophys Res Lett. doi:10.1029/2011GL050520

Goswami BN, Madhusoodanan MS, Neema CP, Sengupta D, (2006) A physical mechanism for North Atlantic SST influence on the Indian summer monsoon. Geophys Res Lett. doi:10.1029/2005GL024803

Gray ST, Graumlich LJ, Betancourt JL, Pederson GT (2004) A tree-ring based reconstruction of the Atlantic Multidecadal Oscillation since 1567 A.D. Geophys Res Lett. doi:10.1029/2004GL019932

Gray LJ, Woolings TJ, Andrews M, Knight J (2016) Eleven-year solar cycle signal in the NAO and Atlantic/European blocking. Q J R Meteorol Soc 142:1890–1903. doi:10.1002/qj.2782

Hajian S, Movahed MS (2010) Multifractal detrended cross-correlation analysis of sunspot numbers and river flow fluctuations. Physica A 389:4942–4957. doi:10.1016/j.physa.2010.06.025

He LY, Chen SP (2011) A new approach to quantify power-law cross-correlation and its application to commodity markets. Physica A 390:3806–3814. doi:10.1016/j.physa.2011.06.013

Huang B, Banzon VF, Freeman E, Lawrimore J, Liu W, Peterson TC, Smith TM, Thorne PW, Woodruff SD, Zhang HM (2015) Extended reconstructed sea surface temperature version 4 (ERSST.v4): part I. Upgrades and intercomparisons. J Clim 28:911–930. doi:10.1175/JCLI-D-14-00006.1

Huang B, Thorne P, Smith T, Liu W, Lawrimore J, Banzon V, Zhang H, Peterson T, Menne M (2016) Further exploring and quantifying uncertainties for extended reconstructed sea surface temperature (ERSST) Version 4 (v4). J Clim 29:3119–3142. doi:10.1175/JCLI-D-15-0430.1

Jiang P, Yu Z, Gautam MR (2013) Pacific and Atlantic Ocean influence on the spatiotemporal variability of heavy precipitation in the western United States. Global Planet Change 109:38–45. doi:10.1016/j.gloplacha.2013.07.004

Jiang H, Muscheler R, Björck S, Seidenkrantz MS, Olsen J, Sha L, Sjolte J, Eiríksson J, Ran L, Knudsen KL, Knudsen MF (2015) Solar forcing of Holocene summer sea-surface temperatures in the northern North Atlantic. Geology. doi:10.1130/G36377.1

Joly M, Voldoire A (2009) Influence of ENSO on the West African monsoon: Temporal aspects and atmospheric processes. J Clim 22:3193–3210 doi:10.1175/2008JCLI2450.1

Joshi MK, Pandey AC (2011) Trend and spectral analysis of rainfall over India during 1901–2000. J Geophys Res. doi:10.1029/2010JD014966

Kang DD, Lee DI, Jung JW (2013) Dynamical characteristics in time series between PM10 and wind speed. In: Proceedings of the international conference on environment, energy, ecosystems and development Seoul Korea: 78–82

Kang IS, No HH, Kucharski F (2014) ENSO amplitude modulation associated with the mean SST changes in the tropical Central Pacific induced by Atlantic Multidecadal Oscillation. J Clim 27:7911–7920. doi:10.1175/JCLI-D-14-00018.1

Kayano MT, Capistrano VB (2014) How the Atlantic multidecadal oscillation (AMO) modifies the ENSO influence on the South American rainfall. Int J Climatol 34(1):162–178. doi:10.1002/joc.3674

Kim S (2015) ppcor: an R package for a fast calculation to semi-partial correlation coefficients. Commun Stat Appl Methods 22(6):665–674. doi:10.5351/CSAM.2015.22.6.665

Knight JR, Folland CK, Scaife AA (2006) Climate impacts of the Atlantic multidecadal oscillation. Geophys Res Lett 33(17). doi:10.1029/2006GL026242

Knudsen MF, Jacobsen BH, Seidenkrantz MS, Olsen J (2014) Evidence for external forcing of the Atlantic multidecadal oscillation since termination of the little ice age. Nat Commun. doi:10.1038/ncomms4323

Kodera K (2004) Solar influence on the Indian Ocean monsoon through dynamical processes. Geophys Res Lett. doi:10.1029/2004GL020928

Kodera K (2005) Possible solar modulation of the ENSO cycle. Pap Meteorol Geophys 55(1/2):21–32. doi:10.2467/mripapers.55.21

Kristoufek L (2015) Measuring correlations between non-stationary series with DCCA coefficient. Phys A 402:291–298. doi:10.1016/j.physa.2014.01.058

Krivova NA, Solanki SK, Unruh YC (2011) Towards a long-term record of solar total and spectral irradiant. J Atmos Sol Terr Phy 73:223–234. doi:10.1016/j.jastp.2009.11.013

Kucharski F, Kang IS, Farneti R, Feudale L (2011) Tropical Pacific response to 20th century Atlantic warming. Geophys Res Lett. doi:10.1029/2010GL046248

Kucharski F, Ikram F, Molteni F, Farneti R, Kang IS, No HH, King MP, Giuliani G, Mogensen K (2015) Atlantic forcing of Pacific decadal variability. Clim Dyn 46(7):2337–2351. doi:10.1007/s00382-015-2705-z

Kugiumtzis D (2000) Surrogate data test on time series. In: Soofi A, Cao L (eds) Modeling and forecasting financial data. Springer, New York, pp 267–282

Kumar KK, Rajagopalan B, Hoerling M, Bates G, Cane M (2006) Unraveling the mystery of Indian monsoon failure during El Niño. Science 314:115–119. doi:10.1126/science.1131152

Lapp SL, Jacques SJM, Elaine BM, David SJ (2012) GCM projections for the Pacific decadal oscillation under greenhouse forcing for the early 21st century. Int J Climatol 32(9):1423–1442. doi:10.1002/joc.2364

Lean J, Beer J, Bradley R (1995) Reconstruction of solar irradiance since 1610: implications for climate change. Geophys Res Lett 22(23):3195–3198. doi:10.1029/95GL03093

Liu W, Huang B, Thorne PW, Banzon VF, Zhang HM, Freeman E, Lawrimore J, Peterson TC, Smith TM, Woodruff SD (2014) Extended reconstructed sea surface temperature Version 4 (ERSST.v4): part II. parametric and structural uncertainty estimations. J Clim 28:931–951. doi:10.1175/JCLI-D-14-00007.1

Lockwood M (2010) Solar change and climate: an update in the light of the current exceptional solar minimum. Proc R Soc A Math Phys 466:303–329. doi:10.1098/rspa.2009.0519

MacDonald GM, Case RA (2005) Variations in the Pacific Decadal Oscillation over the past millennium. Geophys Res Lett. doi:10.1029/2005GL022478

Maher N, McGregor S, England MH, Sen Gupta A (2015) Effects of volcanism on tropical variability. Geophys Res Lett 42:6024–6033. doi:10.1002/2015GL064751

Malik A, Brönnimann S, Stickler A, Raible CC, Muthers S, Anet J, Rozanov E, Schmutz W (2017) Decadal to multi-decadal scale variability of Indian summer monsoon rainfall in the coupled ocean-atmosphere-chemistry climate model SOCOL-MPIOM. Clim Dyn. doi:10.1007/s00382-017-3529-9

Mann ME, Cane MA, Zebiak SE, Clement A (2005) Volcanic and solar forcing of the tropical Pacific over the past 1000 years. J Clim 18:447–456. doi:10.1175/JCLI-3276.1

Mann ME, Zhang Z, Rutherford S, Bradley RS, Hughes MK, Shindell D, Ammann C, Faluvegi G, Ni F (2009) Global signatures and dynamical origins of the little ice age and medieval climate anomaly. Science 326:1256–1260. doi:10.1126/science.1177303

Mantua NJ, Hare SR (2002) The Pacific decadal oscillation. J Oceanogr 58(1):35–44. doi:10.1023/A:1015820616384

Mantua NJ, Hare SR, Zhang Y, Wallace JM, Francis RC (1997) A Pacific interdecadal climate oscillation with impacts on salmon production. Bull Am Meteorol Soc 78:1069–1079. doi:10.1175/1520-0477(1997)078<1069:APICOW>2.0.CO;2

Marinho EBS, Sousa AMYR, Andrade RFS (2013) Using detrended cross correlation analysis in geophysical data. Phys A 392:2195–2201. doi:10.1016/j.physa.2012.12.038

McCabe GJ, Palecki MA, Betancourt JL (2004) Pacific and Atlantic Ocean influences on multidecadal drought frequency in the United States. Proc Natl Acad Sci 101:4136–4141. doi:10.1073/pnas.0306738101

McGregor S, Timmermann A (2011) The effect of explosive tropical volcanism on ENSO. J Clim 24(8):2178–2191. doi:10.1175/2010JCLI3990.1

McGregor S, Timmermann A, Stuecker MF, England MH, Merrifield M, Jin FF, Chikamoto Y (2014) Recent Walker circulation strengthening and Pacific cooling amplified by Atlantic warming. Nature. Clim Change 4:888–892. doi:10.1038/nclimate2330

Meehl GA, Arblaster JM, Matthes K, Sassi F, Loon HV (2009) Amplifying the Pacific climate system response to a small 11-year solar cycle forcing. Science. doi:10.1126/science.1172872

Mehta VM, Lau WKM (1997) Influence of solar irradiance on the Indian monsoon-ENSO relationship at decadal-multidecadal time scales. Geophys Res Lett 24(2):159–162. doi:10.1029/96GL03778

Mo KC, Schemm JE (2008) Relationships between ENSO and drought over the southeastern United States. Geophys Res Lett. doi:10.1029/2008GL0346

Muthers S, Anet JG, Stenke A, Raible C, Rozanov E, Brönnimann S, Peter T, Arfeuille FX, Shapiro AI, Beer J, Steinhilber F, Brugnara Yuri, Schmutz W (2014) The coupled atmosphere-chemistry-ocean model SOCOL-MPIOM. Geosci Model Dev 7(5):2157–2179. doi:10.5194/gmd-7-2157-2014

Muthers S, Raible CC, Rozanov E, Stocker TF (2016) Response of the AMOC to reduced solar radiation—the modulating role of atmospheric chemistry. Earth Syst Dyn 7:877–892. doi:10.5194/esd-7-877-2016

Narashima R, Bhattacharyya S (2010) A wavelet cross-spectral analysis of solar-ENSO rainfall connections in the Indian monsoons. Appl Comput Harmon Anal 28:285–295. doi:10.1016/j.acha.2010.02.005

Newman M (2007) Interannual to decadal predictability of tropical and North Pacific sea surface temperatures. J Clim 20:2333–2356. doi:10.1175/JCLI4165.1

Newman M, Compo GP, Alexander MA (2003) ENSO-forced variability of the Pacific decadal oscillation. J Clim 16(23):3853–3857. doi:10.1175/1520-0442(2003)016<3853:EVOTPD>2.0.CO;2

Newman M, Alexander MA, Ault TR, Cobb KM, Deser C, Di Lorenzo E, Mantua NJ, Miller AJ, Minobeh S, Nakamura H, Schneider N, Vimont DJ, Phillips AS, Scott JD, Smith CA (2016) The Pacific decadal oscillation, revisited. J Clim 29:4399–4427. doi:10.1175/JCLI-D-15-0508.1

Ohba M, Shiogama H, Yokohata T, Watanabe M (2013) Impact of strong tropical volcanic eruptions on ENSO simulated in a coupled GCM. J Clim 26:5169–5182. doi:10.1175/JCLI-D-12-004

Otterå OH, Bentsen M, Drange H, Suo L (2010) External forcing as a metronome for Atlantic multidecadal variability. Nat Geosci 3:688–694. doi:10.1038/ngeo955

Pausata FSR, Chafik L, Caballero R, Battistid DS (2015) Impacts of high-latitude volcanic eruptions on ENSO and AMOC. Proc Natl Acad Sci USA 112(45):13784–13788. doi:10.1073/pnas.1509153112

Piao L, Fu Z, Yuan N (2016) “Intrinsic” correlations and their temporal evolutions between winter-time PNA/EPW and winter drought in the west United States. Sci Rep. doi:10.1038/srep19958

Pierce DW, Barnett TP, Latif M (2000) Connections between the Pacific Ocean tropics and mid-latitudes on decadal timescales. J Clim 13:1173–1194. doi:10.1175/1520-0442(2000)013<1173:CBTPOT>2.0.CO;2

Podobnik B, Stanley HE (2008) Detrended cross correlation analysis: a new method for analyzing two non-stationary time series. Phys Rev Lett. doi:10.1103/PhysRevLett.100.084102

Ramaswamy V, Boucher O, Haigh J, Hauglustaine D, Haywood J, Myhre G, Nakajima T, Shi GY, Solomon S (2001) Radiative forcing of climate change. In: Houghton J, Ding Y, Griggs D et al (eds) IPCC third assessment report: climate change 2001. Cambridge University Press, Cambridge, pp 350–416

Rayner NA, Parker DE, Horton EB, Folland CK, Alexander LV, Rowell DP, Kent EC Kaplan A (2003) Global analyses of sea surface temperature, sea ice, and night marine air temperature since the late nineteenth century. J Geophys Res Atmos. doi:10.1029/2002JD002670

Reichler T, Kim J, Manzini E, Kröger J (2012) A stratospheric connection to Atlantic climate variability. Nat Geosci 5:783787. doi:10.1038/ngeo1586

Schneider N, Cornuelle BD (2005) The forcing of the Pacific decadal oscillation. J Clim 18:4355–4373. doi:10.1175/JCLI3527.1

Shapiro AI, Schmutz W, Rozanov E, Schoell M, Haberreiter M, Shapiro AV, Nyeki S (2011) A new approach to the long-term reconstruction of the solar irradiance leads to large historical solar forcing. Astron Astrophys. doi:10.1051/0004-6361/201016173

Shen C, Wang WC, Gong W, Hao Z (2006) A Pacific Decadal Oscillation record since 1470 AD reconstructed from proxy data of summer rainfall over eastern China. Geophys Res Lett. doi:10.1029/2005GL024804

Steinhilber F, Beer J (2013) Prediction of solar activity for the next 500 years. J Geophys Res 118(5):1861–1867. doi:10.1002/jgra.50210

Stenchikov G, Delworth TL, Ramaswamy V, Stouffer RJ, Wittenberg A, Zeng F (2009) Volcanic signals in oceans. J Geophys Res. doi:10.1029/2008JD011673

Sutton R, Hodson DLR (2007) Climate response to basin-scale warming and cooling of the North Atlantic Ocean. J Clim 20:891–907. doi:10.1175/JCLI4038

Swingedouw D, Ortega P, Mignot J, Guilyardi E, Masson-Delmotte V, Butler PG, Khodri M, Séférian R (2014) Bidecadal North Atlantic ocean circulation variability controlled by timing of volcanic eruptions. Nat Commun. doi:10.1038/ncomms7545

Timmermann A, An SI, Krebs U, Goosse H (2005) ENSO suppression due to weakening of the Atlantic thermohaline circulation. J Clim 18:3122–3139. doi:10.1175/JCLI3495.1

Timmermann A, Okumura Y, An SI, Clement A, Dong B, Guilyardi E, Hu A, Jungclaus JH, Renold M, Stocker TF, Stouffe RJ, Sutton R, Xie SP, Yin J (2007) The influence of a weakening of the Atlantic Meridional Overturning Circulation on ENSO. J Clim 20:4899–4919. doi:10.1175/JCLI4283.1

Vassoler RT, Zebende GF (2012) DCCA cross-correlation coefficient apply in time series of air temperature and air relative humidity. Phys A 391:2438–2443. doi:10.1016/j.physa.2011.12.015

Vimont DJ, Battisti DS, Hirst AC (2001) Footprinting: a seasonal connection between the tropics and midlatitudes. Geophys Res Lett 28:3923–3926. doi:10.1029/2001GL013435

Vimont DJ, Battisti DS, Hirst AC (2003a) The seasonal footprinting mechanism in the CSIRO general circulation models. J Clim 16:2653–2667. doi:10.1175/1520-0442(2003)016<2653:TSFMIT>2.0.CO;2

Vimont DJ, Wallace JM, Battisti DS (2003b) The seasonal footprinting mechanism in the Pacific: implications for ENSO. J Clim 16:2668–2675. doi:10.1175/1520-0442(2003)016<2668:TSFMIT>2.0.CO;2

Visbeck M, Chassignet EP, Curry RG, Delworth TL, Dickson RR, Krahmann G (2003) The ocean's response to North Atlantic oscillation variability. In: Hurrell JW, Kushnir Y, Ottersen G, Visbeck M (eds) The North Atlantic Oscillation: climatic significance and environmental impact. American Geophysical Union, Washington, DC

Wei W, Lohmann G (2012) Simulated Atlantic Multi-decadal Oscillation during the. Holocene J Clim 25:6989–7002. doi:10.1175/JCLI-D-11-00667.1

Wu S, Liu Z, Zhang R (2011) On the observed relationship between the Pacific decadal oscillation and the Atlantic Multidecadal oscillation. J Oceanogr 67:27–35. doi:10.1007/s10872-011-0003-x

Yeh SW, Kirtman BP (2003) On the relationship between the interannual and decadal SST variability in the north Pacific and tropical Pacific Ocean. J Geophys Res. doi:10.1029/2002JD002817

Yuan N, Fu Z, Zhang H, Piao L, Xoplaki E, Luterbacher J (2015) Detrended partial-cross-correlation analysis: a new method for analyzing correlations in complex system. Sci Rep. doi:10.1038/srep08143

Zanchettin D, Timmreck C, Graf HF, Rubino A, Lorenz S, Lohmann K, Krüger K, Jungclaus JH (2012) Bi-decadal variability excited in the coupled ocean-atmosphere system by strong tropical volcanic eruptions. Clim Dyn 39(1–2):419–444. doi:10.1007/s00382-011-1167-1

Zebende G (2011) DCCA cross-correlation coefficient: quantifying level of cross-correlation. Phys A 390:614–618. doi:10.1016/j.physa.2010.10.022

Zhang R, Delworth TL (2006) Impact of Atlantic Multidecadal Oscillations on India/Sahel rainfall and Atlantic hurricanes. GeophysRes Lett. doi:10.1029/2006GL026267

Zhang R, Delworth TL (2007) Impact of Atlantic multidecadal oscillation on north Pacific climate variability. Geophys Res Lett. doi:10.1029/2007GL031601

Zhang L, Wang C (2013) Multidecadal North Atlantic sea surface temperature and Atlantic meridional overturning circulation variability in CMIP5 historical simulations. J Geophys Res Oceans 118:5772–5791. doi:10.1002/jgrc.20390

Zhang Y, Wallace JM, Iwasaka N (1996) Is climate variability over the north Pacific a linear response to ENSO? J Clim 9:1468–1478